

ABSTRACT

Three dimensional imaging set-ups that offers full wavefront reconstruction such as the holographic off-axis configuration are (1) bulky, (2) expensive to build and maintain and (3) sensitive to vibrations. This thesis provides a successful implementation of Digital In-line Holography (DIH) which addresses these issues. Underlying principles of DIH are discussed. A reconstruction program is developed and several parameters such as (1) hologram to object distance, (2) reconstruction distance, (3) background field and (4) wavelength are studied through simulations. The reconstruction algorithm is implemented using experimental data. The wavefront of three samples: (1) regular-shaped objects (spherical glass beads), (2) irregular-shaped objects (lime powder) and (3) biological samples (cheek cells) were obtained. Finally, the reconstruction program is applied for lateral movement measurement and object localization.

CHAPTER I: INTRODUCTION

1.1 BACKGROUND

This thesis mainly offers the basic recipe for digital in-line holography (DIH): (1) a working DIH set-up and (2) a working DIH reconstruction program. The main goal of this thesis is to create digital in-line holograms and be able to successfully reconstruct it. The source of inspiration for this thesis came from the fact that DIH offers a very simple set-up—only a light source, a pinhole and a camera are needed for DIH. With this new working set-up, we are hoping that we may be able to intersect several domains of research in the laboratory to explore new possibilities.

In this thesis, DIH is explored though simulations and experiments. For the simulation, several parameters in the reconstruction algorithm are studied: (1) hologram quality in terms of its distance from the object, (2) the reconstruction distance, (3) effect on the background field and (4) the wavelength used. These simulations were carried out before the implementation on actual objects. For the experiment, the set-up and reconstruction algorithm are used to reconstruct the wavefront of (1) spherical glass beads with average size of 50 μm , (2) irregularly shaped lime powder and (3) biological sample (cheek cells). To further test the set-up, it was also used in axial movement measurement and object localization.

1.2 MOTIVATION

Holographic imaging offers complete wavefront reconstruction (i.e., with phase and intensity maps). The reconstruction of the full wavefront is important in many fields such as

phase microscopy [1], astronomy [2], ophthalmology [3] and shearography [4]. However, conventional set-ups such as that of the off-axis configuration are (1) bulky due to the need of a stable platform (i.e., optical tables) and several components (i.e., beam splitters and mirrors), (2) expensive to build and maintain because of the costly and sensitive components and (3) sensitive to vibrations because the separate beams in off-axis holography must be recombined perfectly in order to produce a good hologram. A set-up that addresses these issues is worthy of exploration.

1.3 STATEMENT OF THE PROBLEM

Using the digital in-line holography (DIH) configuration (i.e., no separate reference beam is used), the proposed setup requires fewer components (laser, pinhole and digital camera). This enables us to create a holography set-up that is compact and inexpensive. Also, since there is no separate holographic reference beam, it is not prone to vibrations. Compared to conventional imaging, sample preparation is minimal because no staining is required for transparent specimens. Near real-time processing can also be done using fast reconstruction algorithms.

Digital in-line holography provides a solution to the presented problems in off-axis holography. DIH provides a compact, inexpensive and insensitive to vibration holographic set-up. In this study, DIH is fully implemented.

1.4 OBJECTIVES AND SCOPE OF THE STUDY

The objectives of this study are as follows:

1. Implement a set-up for Digital In-line Holography
2. Create a reconstruction program for DIH
3. Study the parameters in DIH reconstruction through simulations

4. Reconstruct the wavefront of (1) regular-shaped samples, (2) irregular shaped samples and (3) biological samples.
5. Apply DIH in axial movement measurement and object localization

This study includes the demonstration of DIH, both in simulations and experiments. This also includes the application to lateral movement measurement and object localization. This study utilizes the amplitude of the wavefront and not the phase.

1.5 OUTLINE

The next chapter (Chapter 2) of this thesis discusses several papers on DIH. This shall provide a review of related literature in DIH. Next is Chapter 3 that shall provide the reader an overview of the basic principles in DIH. This includes a sub-chapter on holography which is about the basic mathematical and conceptual foundations in holography. A sub-chapter on the differences in the set-up and images produced in in-line and off-axis holography is also presented. Lastly, an extensive sub-chapter on the formulation of DIH is added which highlights the (1) Fresnel-Huygens principle, (2) the difference between the Fresnel-Kirchoff and Rayleigh-Sommerfeld formulation and lastly (3) Fresnel-Kirchoff formulation where the basis of the reconstruction program for this thesis is based on. The methodology (Chapter 4) and the results and discussions (Chapter 5) follow. For the simulation, the simulated test object is subjected to different reconstruction and hologram formation parameters. As for the experiments, the experimental work is described, holograms captured and their reconstructions are presented. In Chapter 6, we draw some conclusions and discuss possible improvements and further investigations. Appendices with the written code both written in Matlab for simulation and reconstruction is also added.

REFERENCES

1. Phase Microscopy, “<http://www.microscopy-uk.org.uk/mag/artaug02/pjphase.html>”, Accessed: February 20, 2013.
2. J. Primot, G. Rousset, and J. C. Fontanella, "Deconvolution from wave-front sensing: a new technique for compensating turbulence-degraded images," *J. Opt. Soc. Am. A* **7**, 1598- 1608 (1990)
3. J. Liang, B. Grimm, S. Goelz, and J. F. Bille, "Objective measurement of wave aberrations of the human eye with use of a Hartmann-Shack wave-front sensor," *J. Opt. Soc. Am. A* **11**, 1949- (1994)
4. F. C. I. Catalan, A.M.S. Maallo and P. F. Almoro, "Fringe analysis and enhanced characterization of sub-surface defects using fringe-shifted shearograms", *Opt. Com.* (2012), <http://dx.doi.org/10.1016/j.optcom.2012.06.020>

CHAPTER II: REVIEW OF RELATED LITERATURE

In 1947, a new concept for optical imaging known as Holography was invented by Dennis Gabor [1-3]. Originally, Gabor's concept was introduced to overcome the problem of magnetic electron lenses for electron microscopy [4]. Practical implementation of these lenses was a problem due to substantial aberration effects; these lenses were even compared to the 'bottom of a champagne bottle' [5]. Instead of using the lenses, Gabor used a pinhole to produce a spherical wave—an expanding wave which is perfect for magnification. This gave birth to the point source in-line holographic configuration.

Holograms may be recorded and reconstructed photographically or digitally. The introduction of the CCD array opened many doors for holography—skipping the chemical processing and physical reconstruction of the objects. Now, most of holography applications deal with numerical recording and reconstruction because of its ability to record holograms easily, ease of storage, minimal costs, easily repeatable experiments and ease of information transfer thru several media such as the internet. The combination of the digitization of hologram recording and the original idea of Gabor became known as Digital In-line Holography.

One of the literatures that became the backbone of this DIH thesis is a Master's Thesis by Nils Adie [6]. His thesis acted as the first step towards a successful implementation of DIH in extreme ultraviolet radiation. The main conclusion of his thesis is that one harmonic must be isolated in order to receive a clear image. His derivation of the discretized Fresnel-Kirchoff (FK) integral for DIH (similar to that of X.M. Huang et. Al. [7]) is of my greater interest for this study. As with this thesis, he used the FK integral to determine the field in one plane using the field in another plane (i.e., if we know the field in the object plane, then we are able to determine the field in the far-field plane). He then used this

relation in order to conveniently determine the field on the object plane using the hologram plane. The complete derivation is expounded in Chapter 3.3.

The phase reconstruction properties in DIH have not been sufficiently discussed in literature [8]. The latest paper to date about the phase reconstruction in DIH microscopy is presented by A. Nelleri et Al. in 2010 [8]. In their paper, instead of the usual one Fourier transform in the reconstruction, they have used three Fourier transforms. It is shown that the phase reconstruction has improved. However, with the advantages of DIH, further improvement for DIH phase reconstruction is worthy of further research. This thesis provides an initial step in this field by using biological samples with phase attributes.

Several papers have already been published using several applications and different objects in DIH. These include the use DIH in compressive holography [9], measurement of raindrops and snowflakes [10], disease diagnostics [11] and terrestrial and exobiological research [12]. One application that uses numerical focusing for depth perception is presented by T. Khanam et Al. [13] in 2011. In their paper, they have accurately measured the length and orientation of needle-shaped particles in a solution. Just like in the work of Adie, they have used the FK integral for hologram reconstruction in an in-line configuration. They have utilized the focusing effect in in-line holography in order to determine the focused image and in turn, determining the length, location and orientation of the particles. In this thesis, visual inspection utilizing the focusing effect in in-line holography is applied to lateral movement measurement and object localization.

A direction for DIH that is worthy of further research is the exploration of the possibility of the use of different light sources. Several researchers have already used infrared [14] and X-ray [6, 15, 16] for DIH. A paper that needs to be highlighted in terms of the use of other light sources is by L. Repetto et Al. [17] which utilize an LED-based DIH. This is of course is of great advantage since we are able to produce a much smaller holographic set-up and of course a much cheaper DIH set-up. In their paper, the light from a green LED light is

focused using an objective lens. The light is then focused to a $10\mu\text{m}$ pinhole. Using $10\mu\text{m}$ spherical latex spheres, they were able to successfully reconstruct the holograms.

Another direction for DIH that is worthy of further research is the exploration of the reoccurring problem in DIH—the twin-image problem. Because of the in-line configuration, in the observer’s point of view, a focused virtual image is seen with a blurry image of the real image in the background (see Chapter 3.2). One of the papers that have described an iterative algorithm that gives a numerical solution to this problem is by X.M. Huang [7]. However, one drawback of this technique is that it is only applicable to pure amplitude objects. The development of an algorithm that is applicable to phase-type objects is currently in progress.

REFERENCES

1. A.D. Gabor, "A New Microscopic Principle", Nature 161, 777-B (1948).
2. A.D. Gabor, "Microscopy by Reconstructed Wave-Fronts", Proc. Royal Soc. of London 197(1051), 454–487 (1949).
3. A. D. Gabor, "Microscopy by Reconstructed Wave Fronts: II", Proc. Phy. Soc. 64(449), (1951).
4. S.F. Johnston, "From white elephant to Nobel Prize: Dennis Gabor's wavefront reconstruction", Historical Studies in the Physical and Biological Science 36 (1), pp.35-70 (2005).
5. P. Ferraro et al. (eds.), Coherent Light Microscopy, Springer Series in Surface Sciences 46, DOI 10.1007/978-3-642-15813-1_1
6. N. Adie, "Digital in-line holography with extreme ultraviolet radiation", Master's Thesis, Lund Reports on Atomic Physics, LRAP-334, August 2005.
7. X. Huang, J. Zuo and J. Spence, "Wavefront reconstruction for in-line holograms formed by pure amplitude object", Applied Surface Science Vol.148, 1999.
8. A. Nelleri, J. Joseph and K. Singh, "Phase reconstruction in lensless digital in-line holographic microscopy", Optics and Laser in Engineering 48, pp. 27-31 (2010).
9. D. Brady, K. Choi, D. L. Marks, R. Horisaki and S. Lim, "Compressive Holography", 17 (15) pp.13040-13049 (2009).
10. H. Vössing and S. Borrman, "In-line holography of cloud volumes applied to the measurement of raindrops and snowflakes", Atmospheric Research 49, 199–212, (1998)
11. S. Hugo, T. Naidoo, H. Swart, S. Potgieter, P.V. Rooyen, and K. Land, "A lensless , automated microscope for disease diagnostics", SAIEE 103(1), 48–54 (2012).
12. S.K. Jericho, P. Klages, J.Nadeau, E.M. Dumas, M.H. Jericho and H.J. Kreuzer, "In-line digital holographic microscopy for terrestrial and exobiological research", Planetary and Space Sceince 58 pp. 701-705 (2010).
13. T. Khanam, M. Rahman, A. Rajendran, V. Kariwala and A. Asundi, "Accurate size measurement of needle-shaped particles using digital holography", Chemical Engineering Science 66, pp. 2899-2706 (2011).
14. L. Repetto, R. Chittofrati, E. Piano and C. Pontiggia, "Infrared lensless holographic microscope with vidicon camera for inspection of metallic evaporation on silicon wafers", Opt. Com. 251 pp. 44-50 (2005).
15. E. Mengotti and G. Genound, "Towards time-resolved X-UV digital in-line holography", Master's Thesis, Lund Reports on Atomic Physics, LRAP-368, (2006).

16. R. Heine, T. Gorniak, T. Nisius, C. Christophis, M.E. Pettitt, F. Staier, T. Wilhein, S. Rehbein, M. Grunze, A. Roschahn, “Digital in-line X-ray holography with zone plates”, Ultramicroscopy 111, pp. 1131-1136 (2011).
17. L. Repetto, E. Piano and C. Pontiggia, “Lenless digital holographic microscope with light-emitting diode illumination”, Opt. Letters 29 (10) pp.1132-1133 (2004).

CHAPTER III: PRINCIPLES

3.1 HOLOGRAPHY

Basically, holography uses the interference of two coherent beams: (1) an object beam which is the scattered wave from an object and (2) a reference beam which is the beam which is directed to the recording medium without being distorted. The complex amplitude of these two beams can be written as:

$$O(x, y) = o(x, y)e^{i\varphi_o(x, y)} \quad (3.1)$$

$$R(x, y) = r(x, y)e^{i\varphi_r(x, y)} \quad (3.2)$$

Where o and r are the real amplitudes of the object and reference wave, respectively. The value $\varphi_o(x, y)$ and $\varphi_r(x, y)$ are the phases of the object and reference wave, respectively. The interference pattern of these beams is recorded and is regarded as the hologram. When reference beam is shone to the hologram, the depth of focus and effects of perspective of the original object are manifested. Combining them mathematically yields the intensity of the hologram given by:

$$I(x, y) = |O(x, y) + R(x, y)|^2 \quad (3.3)$$

$$\begin{aligned} &= R(x, y)R^*(x, y) + O(x, y)O^*(x, y) + O(x, y)R^*(x, y) + \\ &\quad R(x, y)O^*(x, y) \end{aligned} \quad (3.4)$$

$$I(x, y) = r^2(x, y) + o^2(x, y) + [O(x, y)R^*(x, y) + R(x, y)O^*(x, y)] \quad (3.5)$$

The first term is the intensity of the reference wave while the second term is the intensity of the object wave. The last two terms in the square bracket are the interference

between the two waves. This is called the holographic diffraction. This is the basis of holography.

3.2 OFF-AXIS VERSUS IN-LINE HOLOGRAPHY

3.2.1 OFF-AXIS HOLOGRAPHY

The basic set-up for off-axis holography is illustrated in Figure 1. The reference and the object beam are in a completely different axis hence the terms ‘off-axis’. The beams must be recombined perfectly in order to create a good hologram. With this, the set-up becomes very sensitive to vibrations which for some applications are problematic. However, in some areas this ‘problem’ is being turned into a useful technique for the measurement of the sensitivity of the set-up [1]. This is called interferometric holography. [2]

In off-axis holography, the observer sees the separate real and the virtual image. The angle between the beams causes the images to look separated [3]. This enables the observer to completely block-off the unfocused image. This is the major advantage of off-axis holography in comparison with in-line holography as we shall see in the later section.

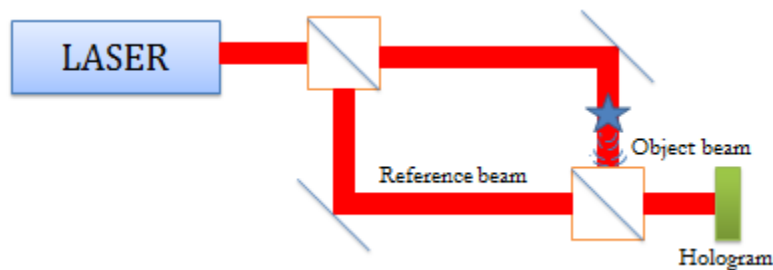


Figure 3.1. Basic Set-up for an off-axis holography configuration.

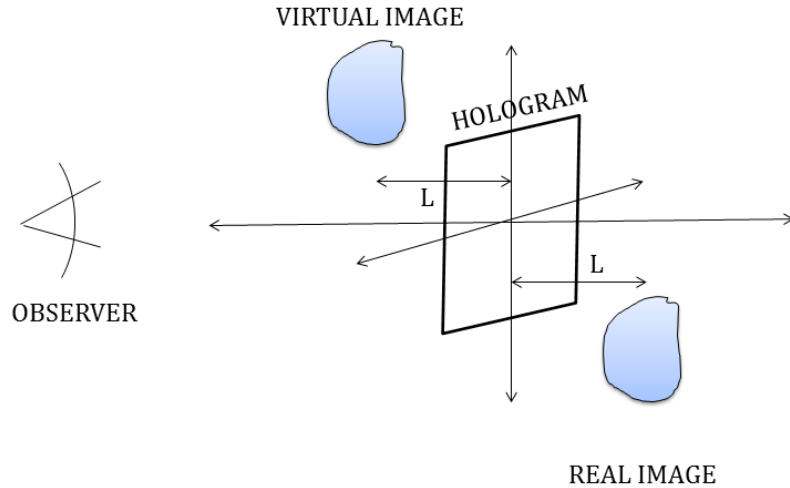


Figure 3.2. Schematic Diagram of how the virtual and real image is seen in off-axis holography.

3.2.2 IN-LINE HOLOGRAPHY

The in-line holography set-up is based on Dennis Gabor's original idea of holography [4-6]. The basic set-up for in-line holography is presented in Figure 3.3. The reference beam and the object beam are in one line hence the term 'in-line'. Figure 3.3a shows Gabor's original idea. The plane wave enters a pinhole with the size close to its wavelength and then a spherical wave is produced. This beam is divergent and the interference of the reference and object beam is subjected to geometric magnification [3]. This is concisely called as the Point Source In-line Holography. This thesis employs this in-line set-up. This set-up should be set apart to the Parallel or Collimated Beam In-line Holography as seen in Figure 3.3b. The main difference of this set-up with the previous one is that it utilizes a plane wave for object illumination. The In-line set-up only uses a single beam which in turn brings stability to the whole set-up. Unlike in off-axis holography, expensive optical tables to prevent unwanted vibrations are not required.

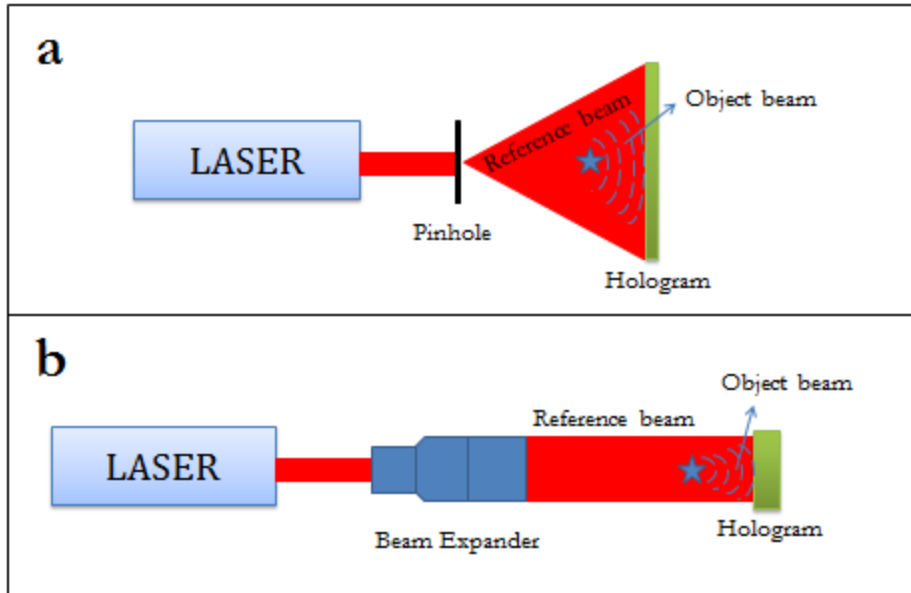


Figure 3.3. Basic Set-up for an in-line holography configuration. (a) Point-source digital in-line holography configuration and (b) Parallel or Collimated beam in-line holography configuration. The set-up in (a) is employed in this thesis.

One major drawback in in-line holography is the alignment of the virtual image and the real image as seen in Figure 3.4. In the observer's point of view, if we are looking at the focused virtual image, a blurry real image is seen in the background. This problem has already been identified by Gabor as seen in his early papers [4-6]. It is impossible to separate the virtual and real image—a problem known as the twin-image problem.

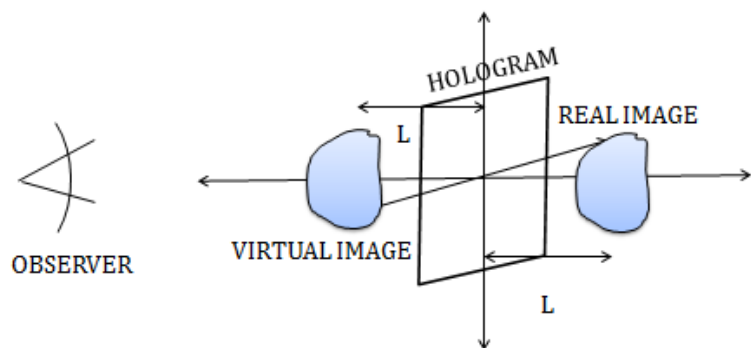


Figure 3.4. Schematic Diagram of how the virtual and real image is seen in off-axis holography.

3.3 DIGITAL IN-LINE HOLOGRAPHY FORMULATION

3.3.1 HUYGENS-FRESNEL PRINCIPLE

Digital In-line Holography (DIH) utilizes the Fresnel-Kirchoff formulation for hologram reconstruction [2, 3, 7-12]. The basis of this mathematical formulation is the Huygens-Fresnel principle which tells us that every point on a propagating wavefront A serves as a source of secondary spherical wavelets for wavefront B. The interference of the secondary wavelets from the different points in Plane A is used to determine the wavefront B [13]. The illustration of this principle is seen in Figure 3.5.

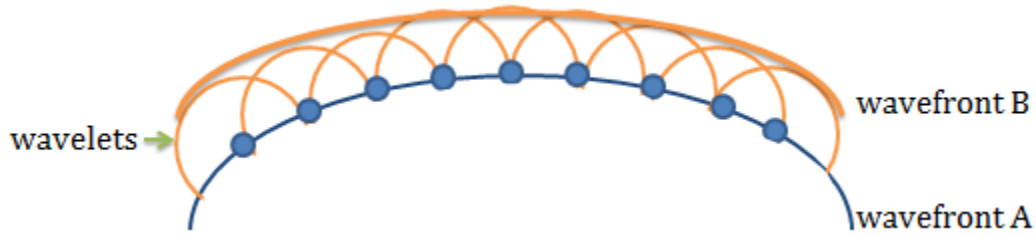


Figure 3.5. Illustration of the Huygens-Fresnel principle which states that every point in wavefront A emits spherical wavelets and the interference of those wavelets forms the wavefront B.

This principle is used in holography by inversion—using the wavefront B (the hologram) to reconstruct wavefront A (the object). Back propagation of the scattered wavefront B which contains information on both the amplitude and phase of the original object that scattered the light wave is utilized.

3.3.2 FRESNEL-KIRCHOFF VERSUS RAYLEIGH-SOMMERFELD FORMULATION

In general, the Fresnel-Kirchoff (FK) and the Rayleigh-Sommerfeld (RS) formulation can be written as [14]:

$$U(P_o) = \frac{A}{j\lambda} \iint \frac{\exp[jk(r_{21}+r_{01})]}{r_{21}r_{01}} \psi ds \quad (3.6)$$

With the FK formulation when

$$\psi = \frac{\cos(\vec{n}, \vec{r}_{01}) - \cos(\vec{n}, \vec{r}_{21})}{2} \quad (3.7)$$

And the RS formulation, with the first and second solution when

$$\psi = \cos(\vec{n}, \vec{r}_{01}) \quad (3.8)$$

$$\psi = -\cos(\vec{n}, \vec{r}_{21}) \quad (3.9)$$

Where the A is the amplitude of the wave, λ is the wavelength of the light used, j is the imaginary number and k is the wavenumber. Other notations in the equations are seen in Figure 3.6. The figure shows a point source illumination of a plane screen where P_2 is the illumination point source, P_1 is aperture point and the P_0 is the observation point.

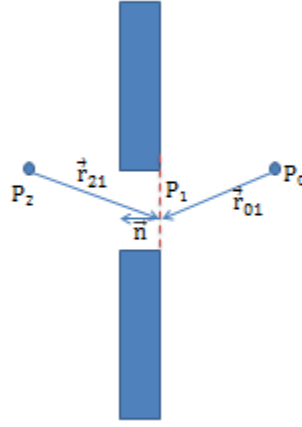


Figure 3.6. Point source illumination of a plane screen.

It must be noted that the FK formulation holds only for an illumination consisting of a single point source. It restricted to the case of an aperture illumination consisting of a single expanding spherical wave. This limitation is removed by the RS formulation [14].

In a paper by Wolf and Marchand in 1964 compared the FK and RS formulation [15]. They have shown that if the linear dimensions of the aperture are large compared with

the wavelength, the FK and RS formulation essentially predicts the same behaviour for the diffracted field in the far or Fraunhofer zone. However, for DIH it must be noted that since the distance between the object plane and hologram plane is small, it must be considered as Fresnel or near-field diffraction [11].

Another paper that compares the FK and RS formulation is by Heurtley in 1973 [16]. In his paper, he has shown that for divergent spherical waves, in the case of diffraction by a circular aperture, the three formulations (positive and negative RS solutions and the FK solutions) marked different behaviour for observation points lying close to the diffracting object. For all distances behind the aperture, the difference between the theories is notable only when the observation point is close to the aperture.

Therefore, the use of the FK formulation is favourable than the RS formulation due to the following reasons:

- (1) RS formulation requires the diffracting screen to be planar while FK formulation does not [14]. Since DIH utilizes a spherical wave for diffraction, FK is preferred.
- (2) RS formulation differs from the FK formulation only when the observation point is close to the aperture [16]. Since the FK formulation is designed for near-field [11], FK is preferred.
- (3) FK is restricted to the case of an aperture illumination consisting of a single expanding spherical wave [14].

3.3.3 FRESNEL-KIRCHHOFF FORMULATION

From Equation 3.6 and 3.7, the FK formulation may be written as:

$$U(P_o) = \frac{1}{j\lambda} \iint U'(P_1) \frac{\exp(jkr_{01})}{r_{01}} ds \quad (3.10)$$

Where

$$U'(P_1) = \left[\frac{A \exp(jkr_{12})}{r_{12}} \right] \left[\frac{\cos(\vec{n}, \vec{r}_{01}) - \cos(\vec{n}, \vec{r}_{21})}{2} \right] \quad (3.11)$$

$U'(P_l)$ describes the secondary sources that have certain amplitudes and phases which can relate the illuminating wavefront and the angles of illumination and observation [14]. For simplicity, we choose to use $r_{0l} \rightarrow -r$ and for illustration purposes, we use Figure 3.7. as a basis for the notations used.

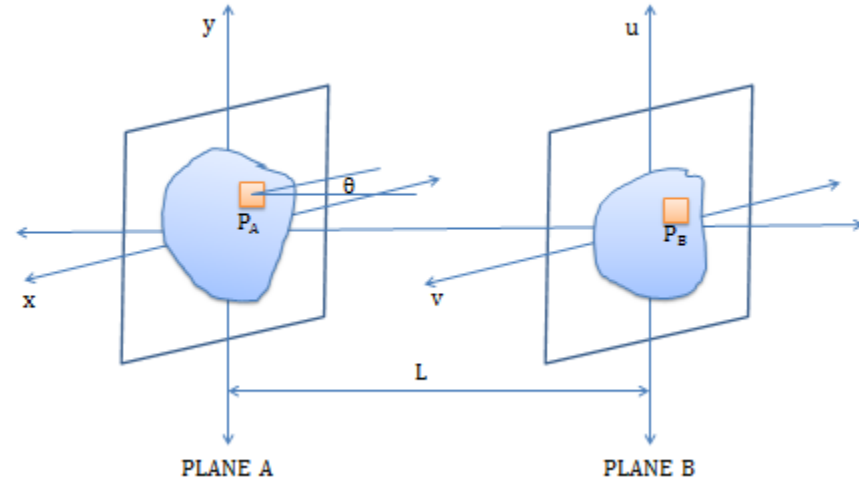


Figure 3.7. Notation used for the Fresnel-Kirchoff formulation.

Therefore, the FK equation is written as [2,3]:

$$U(u, v) = \frac{j}{\lambda} \iint U'(x, y) \frac{\exp(-jkr)}{r} dx dy \quad (3.12)$$

Now, we simplify the equation above using the paraxial approximation. This is when θ is small such that $\cos\theta \approx 1$. Using Figure 3.7, we know that the distance from a point in Plane A to Plane B is

$$r = \sqrt{L^2 + (x - u)^2 + (y - v)^2} \quad (3.13)$$

Isolating L,

$$r = L \sqrt{1 + \frac{(x-u)^2}{L^2} + \frac{(y-v)^2}{L^2}} \quad (3.14)$$

Now by paraxial approximation, we use Taylor Series [8],

$$r = L \left[1 + \frac{(x-u)^2}{2L^2} + \frac{(y-v)^2}{2L^2} + \dots \right] \quad (3.15)$$

Neglecting higher order terms, r becomes

$$r \approx L + \frac{x^2+y^2}{2L} + \frac{u^2+v^2}{2L} - \frac{(xu+yv)}{L} \quad (3.16)$$

Putting this value in the FK formulation:

$$U(u, v) = \frac{j}{\lambda} \iint U'(x, y) \frac{\exp\left[-jk\left(L + \frac{x^2+y^2}{2L} + \frac{u^2+v^2}{2L} - \frac{(xu+yv)}{L}\right)\right]}{L} dx dy \quad (3.17)$$

Note the all the four terms are substituted to the \exp function since this is the phase factor—the value varies fast while only the first term L is substituted to the amplitude factor since its value does not vary fast. Rewriting Equation 3.12,

$$U(u, v) = \frac{j}{\lambda L} e^{-jkl} e^{-jk\frac{u^2+v^2}{2L}} \iint U'(x, y) \exp\left[-jk\left(\frac{x^2+y^2}{2L} - \frac{(xu+yv)}{L}\right)\right] dx dy \quad (3.18)$$

We shall now define:

$$F(x, y) = U'(x, y) \exp\left(-jk\frac{x^2+y^2}{2L}\right) \quad (3.19)$$

Equation (3.17) now becomes:

$$U(u, v) = \frac{j}{\lambda L} e^{-jkl} e^{-jk\frac{u^2+v^2}{2L}} \iint F(x, y) \exp\left[jk\left(\frac{xu+yv}{L}\right)\right] dx dy \quad (3.20)$$

$$U(u, v) = \frac{j}{\lambda L} e^{-jkl} e^{-jk\frac{u^2+v^2}{2L}} \tilde{F}\left(\frac{ku}{2\pi L}, \frac{kv}{2\pi L}\right) \quad (3.21)$$

Where \tilde{F} is the Fourier transform of F . This equation shall be used as a basis for defining different planes of observation.

We shall define three planes: (1) Object plane, (2) Hologram plane and (3) a Far-field plane. Figure 3.8 shows the configuration of these three planes. From Equation 3.21 we know that one plane can be used in order to determine the field at another plane.

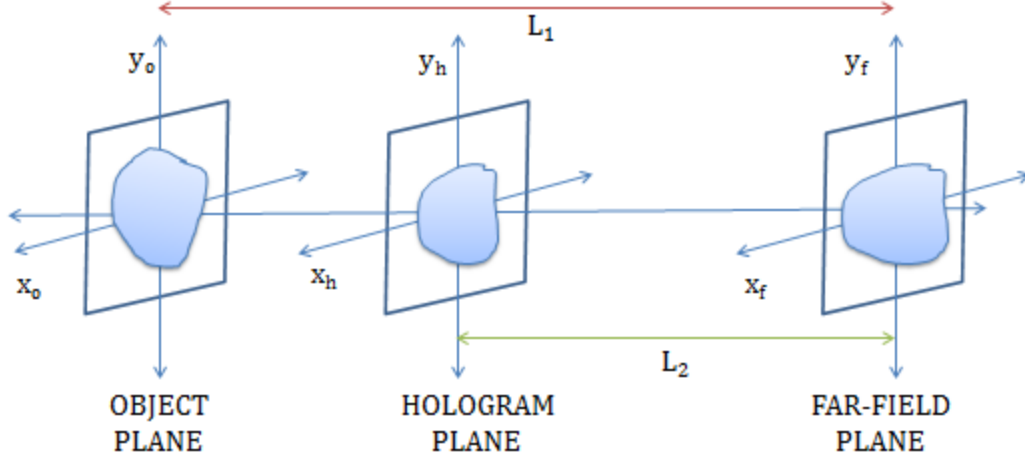


Figure 3.8. Configuration of the Object plane, Hologram plane and the far-field plane.

Using Equation 3.21, we can determine the field in the far field plane using either the object plane or the hologram plane. In equation form, we may write this respectively as:

$$U_f(x_f, y_f) = \frac{j}{\lambda L_1} e^{-j k L_1} e^{-jk \frac{x_f^2 + y_f^2}{2L_1}} \tilde{F}_o\left(\frac{kx_f}{2\pi L_1}, \frac{ky_f}{2\pi L_1}\right) \quad (3.22)$$

$$U_f(x_f, y_f) = \frac{j}{\lambda L_2} e^{-j k L_2} e^{-jk \frac{x_f^2 + y_f^2}{2L_2}} \tilde{F}_H\left(\frac{kx_f}{2\pi L_2}, \frac{ky_f}{2\pi L_2}\right) \quad (3.23)$$

Since Equation 3.22 and 3.23 are equal, we may equate both equations. Therefore, the Fourier transform of the object plane may be written as:

$$\tilde{F}_o\left(\frac{kx_f}{2\pi L_1}, \frac{ky_f}{2\pi L_1}\right) = \frac{\frac{j}{\lambda L_2} e^{-j k L_2} e^{-jk \frac{x_f^2 + y_f^2}{2L_2}}}{\frac{j}{\lambda L_1} e^{-j k L_1} e^{-jk \frac{x_f^2 + y_f^2}{2L_1}}} \tilde{F}_H\left(\frac{kx_f}{2\pi L_2}, \frac{ky_f}{2\pi L_2}\right) \quad (3.24)$$

$$\tilde{F}_o\left(\frac{kx_f}{2\pi L_1}, \frac{ky_f}{2\pi L_1}\right) = \frac{L_1}{L_2} e^{-jk(L_2 - L_1)} e^{-ik \frac{x_f^2 + y_f^2}{2} (\frac{1}{L_2} - \frac{1}{L_1})} \tilde{F}_H\left(\frac{kx_f}{2\pi L_2}, \frac{ky_f}{2\pi L_2}\right) \quad (3.25)$$

Using the definition in Equation (3.19), the hologram plane is isolated:

$$U_o(x_o, y_o) = e^{jk \frac{x_o^2 + y_o^2}{2L_1}} F_O(x_o, y_o) \quad (3.26)$$

$$U_o(x_o, y_o) = e^{jk\frac{x_o^2+y_o^2}{2L_1}} FT^{-1} \left\{ \tilde{F}_o \left(\frac{kx_f}{2\pi L_1}, \frac{ky_f}{2\pi L_1} \right) \right\} \quad (3.27)$$

Combining Equation (3.25) to Equation (3.27),

$$U_o(x_o, y_o) = e^{jk\frac{x_o^2+y_o^2}{2L_1}} FT^{-1} \left\{ \frac{L_1}{L_2} e^{-jk(L_2-L_1)} e^{-ik\frac{x_f^2+y_f^2}{2}(\frac{1}{L_2}-\frac{1}{L_1})} \tilde{F}_H \left(\frac{kx_f}{2\pi L_2}, \frac{ky_f}{2\pi L_2} \right) \right\} \quad (3.28)$$

This equation is the ‘recipe’ for the reconstruction in in-line holography [3,17,18].

However, in digital holography only the intensity is recorded on the hologram plane. Therefore, $U_h(x_h, y_h)$ cannot be used; the value of the recorded intensity used instead: $\sqrt{I_h(x_h, y_h)}$. The hologram that needs to be Fourier transformed becomes:

$$\tilde{G}_H(x_h, y_h) = FT \left\{ e^{-jk\frac{x_h^2+y_h^2}{2L_2}} \sqrt{|E_h(x_h, y_h)|^2} \right\} \quad (3.29)$$

The FK reconstruction algorithm then becomes:

$$U_o(x_o, y_o) = e^{jk\frac{x_o^2+y_o^2}{2L_1}} FT^{-1} \left\{ \frac{L_1}{L_2} e^{-jk(L_2-L_1)} e^{-ik\frac{x_f^2+y_f^2}{2}(\frac{1}{L_2}-\frac{1}{L_1})} \tilde{G}_H \left(\frac{kx_f}{2\pi L_2}, \frac{ky_f}{2\pi L_2} \right) \right\} \quad (3.30)$$

Since we are only using the intensity of the hologram plane, phase information is partially lost in the reconstruction.

REFERENCES

1. U. Schnars and W. P. O. Jüptner, "Digital recording and numerical reconstruction of holograms", Meas. Sci. Technol. 13 R85-R101 (2002).
2. E. Mengotti and G. Genound, "Towards time-resolved X-UV digital in-line holography", Master's Thesis, Lund Reports on Atomic Physics, LRAP-368, September 2006.
3. N. Adie, "Digital in-line holography with extreme ultraviolet radiation", Master's Thesis, Lund Reports on Atomic Physics, LRAP-334, August 2005.
4. A.D. Gabor, "Microscopy by Reconstructed Wave-Fronts", Proc. Royal Soc. of London 197(1051), 454–487 (1949).
5. A.D. Gabor, "Microscopy by Reconstructed Wave-Fronts", Proc. Royal Soc. of London 197(1051), 454–487 (1949).
6. A. D. Gabor, "Microscopy by Reconstructed Wave Fronts: II", Proc. Phy. Soc. 64(449), (1951).
7. Y. Yang and B. Kang, "Determination of depth-of-focus in lensless in-line digital particle holography", Optik 122, pp 1552-1557, May 2010.
8. S. Lai, B. King and M. Neifeld, "Wave front reconstruction by means of phase-shifting digital in-line holography", Optics Communications 173, pp 155-160, October 1999.
9. W. Zhou, Q. Xu, Y. Yu and A. Asundi, "Phase-shifting in-line digital holography on a digital micro-mirror device", Optics and Laser Engineering 47, pp 896-901, May 2009.
10. T. Khanam, M. Rahman, A. Rajendran, V. Kariwala and A. Asundi, "Accurate size measurement of needle-shaped particles using digital holography", Chemical Engineering Science 66, pp 2899-2706, March 2011.
11. A. Ayoub and S. Tókés, "Digital in-line holographic microscope algorithms for micro-organisms detection and three dimension tracking", Accessed at:
<http://colleges.ksu.edu.sa/Papers/Papers/b25.pdf>
12. S. Hugo, T. Naidoo, H. Swart, S. Potgeiter, P. van Rooyen and K. Land, "A lensless, automated microscope for disease diagnostics", South African Institute of Electrical Engineers Vol. 103(1), pp 48-54, March 2012.
13. E. Hecht, "Optics 4th ed.", Pearson Education Inc., 2002.
14. J. Goodman, "Introduction to Fourier Optics 2nd ed.", McGraw Hill Companies Inc., 1996.
15. E. Wolf and E. Marchand, "Comparison of the Kirchoff and the Rayleigh-Sommerfeld theories of diffraction at an aperture", Journal of the Optical Society of America Vol. 54(5), pp 587-594, May 1964.
16. J. Heurtley, "Scalar Rayleigh-Sommerfeld and Kirchoff diffraction integrals: A comparison of exact evaluations for axial points", Journal of the Optical Society of America Vol. 63(5), pp 1003-1006, May 1973.

17. X. Huang, J. Zuo and J. Spence, "Wavefront reconstruction for in-line holograms formed by pure amplitude object", Applied Surface Science Vol.148, 1999.
18. I. Yamaguchi, J. Kato, S. Ohta and J.Mizuno, "Image formation in phase shifting digital holography and applications to microscopy", Applied Optics, Vol.40 No.34, 2001.

CHAPTER IV: METHODOLOGY

4.1 SIMULATIONS

4.1.1 TEST OBJECT

Before implementing the code written based on Equation 3.30 on actual objects, several simulations are carried out in order to determine the effects of several parameters. The parameters studied include hologram quality in terms of its distance from the object, the reconstruction distance, effect on the background and the wavelength used.

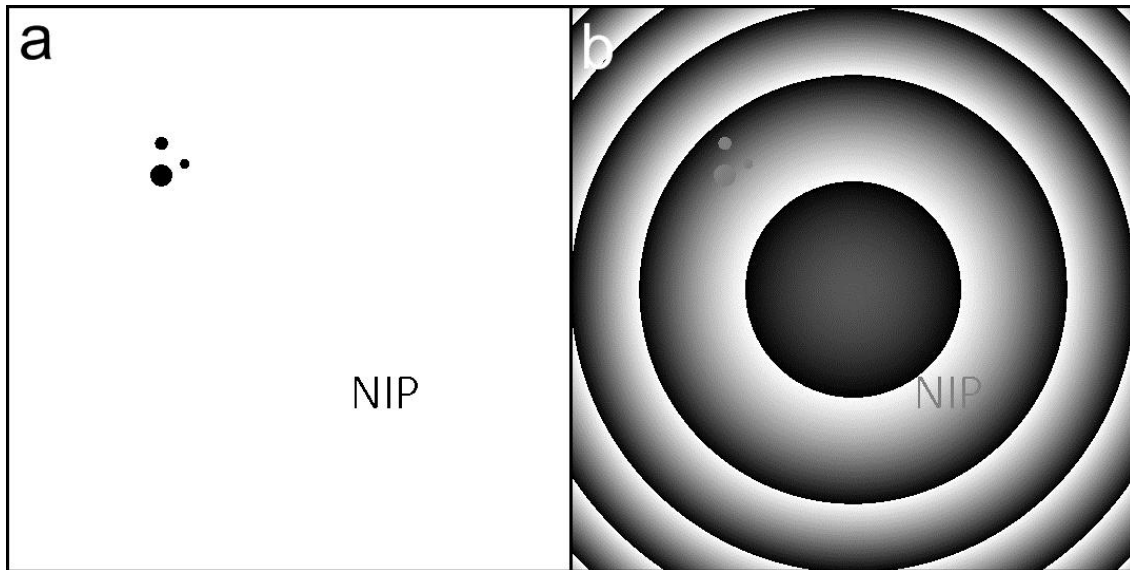


Figure 4.1. The test object. An input object is created using Paint (Amplitude part) and Matlab (Phase part). The amplitude and the phase of the test object are plotted in (a) and (b), respectively.

Figure 4.1 shows the test object used in the simulation. An amplitude object (532 x 532 pixel) was created using Paint Version 6.1 built in Windows 7 Premium (Figure 4.1a) while the phase of the object simulated using MatLab (Figure 4.1b). The object NIP in the lower right corner was selected because of the several curves and lines in its lettering. The effect of the shape of an object is not fully known in reality so an object with variable lateral

dimension such as NIP is chosen. The dots in the upper left corner are selected because several papers in Digital In-Line Holography (DIH) use circular beads as objects. This allows us to counter-check the simulated results with literature values and images.

The objects were chosen to be small in comparison with the background because this makes the holographic diffraction dominant [1]. This is vital in DIH since we want that the object to block out only a small part of the reference wave.

In Figure 4.1, the input object was added with a complex field (reference) in order to have a full complex wave for the object. The field of the object is displayed as amplitude (Figure 4.1a) and as a phase (Figure 4.1b). In this thesis, several parameters in the reconstruction algorithm are studied. These are as follows:

1. HOLOGRAMS

The reverse of equation 3.30 has been implemented in MatLab. We simulate how a hologram will look like given the field in the object plane. In this section, the distance between the object plane and the hologram plane is varied (see Figure 3.4). The quality of the holograms is assessed.

2. RECONSTRUCTION DISTANCE

Using one of the hologram created in the previous section, the object field is reconstructed at different planes. A hologram is created at 15mm from the object plane. The reconstructed field is expected to focus at the distance where the hologram is captured. This focusing effect is vital in applications such as object localization and lateral movement measurement.

3. BACKGROUND FIELD

In this section, the background field is varied: (1) with a plane wave with no tilt, (2) with a plane wave with tilt and (3) with a spherical wave. To assess the quality of the

reconstructed wave, a line scan is implemented. This enables us to qualitatively determine the effect of the background field. The degree of aberration of the spherical wave is varied in order to qualitatively determine its effect on the reconstruction of the hologram.

4. WAVELENGTH

The holograms are simulated and reconstructed at different wavelength values. The analysis shall have two parts: (1) the wavelength is varied in the creation of the hologram (400-700nm); the same wavelength used in reconstruction of the hologram, and (2) the hologram is created at a certain wavelength (500nm); the wavelength is varied in the reconstruction of hologram (400-700nm). The former shall predict how the reconstructed DIH holograms react with different light sources. The effect of the use of UV to infrared light is determined.

4.2 EXPERIMENTS

4.2.1 INSTRUMENTATION

Figure 4.2 shows the DIH set-up. A $25\text{ }\mu\text{m}$ pinhole is utilized in the experiment. The $25\mu\text{m}$ pinhole is the optimal pinhole available. The smaller pinhole ($10\mu\text{m}$) is too small that very little light passes through it. On the other hand, the bigger pinhole ($50\mu\text{m}$) is too large that the light that passes through is too bright. The camera used is a CMOS camera, Optics Star, $1280(\text{H}) \times 1024(\text{V})$, $5.2\text{ }\mu\text{m} \times 5.2\text{ }\mu\text{m}$ pixel size. For this thesis, the light source used is a He-Ne laser ($\lambda = 632.8\text{ nm}$). Because of the limited battery power of a compact laser, we have utilized a separate He-Ne laser. A compact laser or an LED flash light may be utilized for a compact and table-top set-up as seen in Figure 4.3.

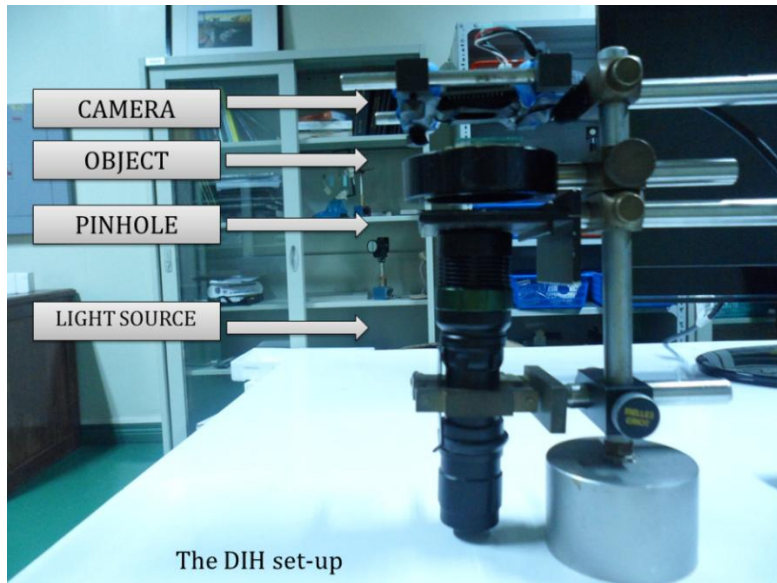


Figure 4.2. DIH experimental set-up.

4.2.2 OBJECTS USED

Three objects were used in this thesis: (1) regular shaped glass beads (spherical with average diameter of $50\mu\text{m}$), (2) irregularly shaped lumps of lime powder and (3) biological samples (cheek cells). The first object was selected because of the regularity of its shape and also, its average diameter is known. Several papers in DIH have used spherical beads as their object and we believe that the use of such object provides a reference for comparison. The second object is selected to extend DIH for irregularly shaped objects. Lastly, the third object is selected to extend DIH for biological samples. The third sample also has some phase components, a field in DIH that has not much been tackled as mentioned in Chapter 2.

4.2.3 AXIAL MOVEMENT MEASUREMENT

The schematic diagram of the DIH set-up is presented in Figure 4.3. The CCD array captures the hologram, which is the interference of the reference and object beam. Using equation 3.30, the object wave front is reconstructed using the hologram captured and the parameters used. The spherical beads that acted as the object are placed at a certain distance

Z_A . At this distance, the hologram is captured by the CCD array. Next, the spherical beads are then moved at a certain distance Δz . The hologram of the glass beads at this distance Z_B is captured.

To determine the axial movement Δz of the spherical beads, the hologram captured with distances Z_A and Z_B are reconstructed at different planes. The value where the reconstruction focuses is regarded as the plane where the object is located. The difference between the distances used to focus the reconstruction in Z_A and Z_B is regarded as the axial movement of the object.

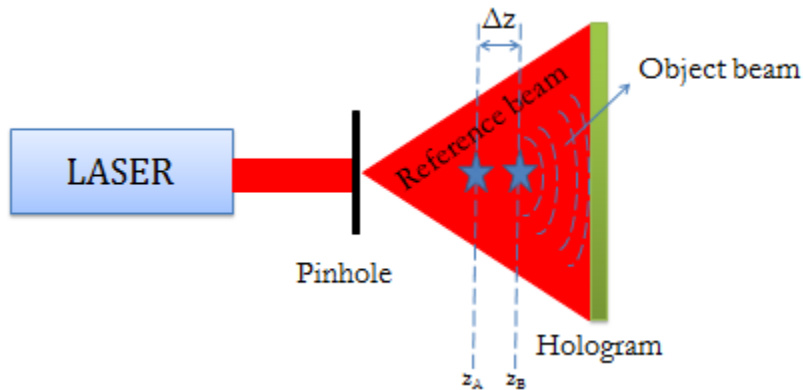


Figure 4.3. A pinhole produces a cone-shaped reference beam. An object on its path blocks the beam, and the diffracted beam is now called the object beam. The interference of the reference and the object beam produces the hologram and is captured by the CCD array. In the diagram, the object is moved at a certain distance Δz . Numerical focusing of the reconstructed hologram is used to determine this distance Δz .

4.2.4 OBJECT LOCALIZATION

Figure 4.4 shows the set-up for object localization. The spherical beads are placed at a certain distance Z_B while the cheek cells are placed at a certain distance Z_A . Unlike in axial movement measurement, only one hologram is captured. This hologram is reconstructed at different planes. In theory, there must be at least two planes where there will be a focused image. The first one is at distance Z_A where the cheek cells are located and Z_B where the spherical beads are located. Through visual inspection of the focused planes, the relative location of the cheek cells and the spherical beads is determined.

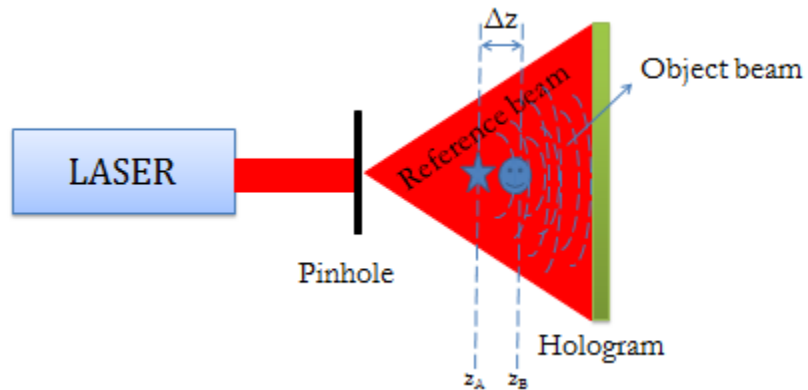


Figure 4.4. Schematic diagram for object localization. The cheek cells are placed at a distance Z_A while the spherical beads are placed at a distance Z_B . A hologram is captured and the distances of the reconstruction where it produces a focused image (one for the cheek cells and one for the spherical beads) is determined.

REFERENCE

1. P. Ferraro et al. (eds.), Coherent Light Microscopy, Springer Series in Surface Sciences 46, DOI 10.1007/978-3-642-15813-1_1

CHAPTER V: RESULTS AND DISCUSSION

5.1 SIMULATIONS

5.1.1 HOLOGRAMS

Figure 5.1 shows the simulated holograms using the reverse of equation 3.30. The wavelength used is 632.8 nm, the camera pixel size is 5.2 μ m by 5.2 μ m and the distance of the far field plane to the object plane is 1m. First we counter-check the simulated holograms if they are similar to the DIH holograms in literature. Two papers have used spherical shaped objects for DIH (L. Repetto et Al. which uses a lens-less LED based DIH microscope [1] and L. Denis et Al. which use a technique for the numerical suppression of the twin-image in DIH [2]). Comparing the hologram of the dots in the upper left corner of Figure 5.1, the simulated holograms are similar to that of holograms in literature.

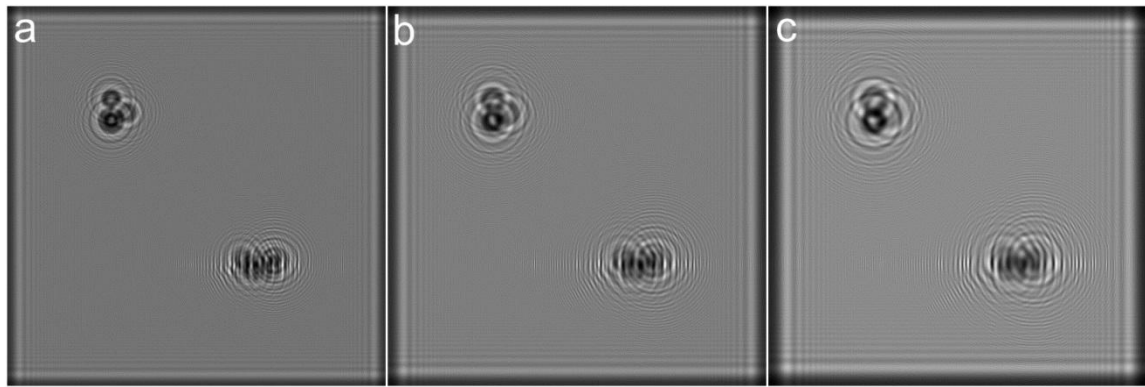


Figure 5.1. Simulated DIH holograms at 10mm, 15mm and 20mm from the object plane.

From Figure 5.1, it is inferred that as the distance of the hologram plane to object plane is decreased, the diffraction pattern produced by the objects decreases in area (the number of fringes decreases). This is expected since as the CCD array (see Figure 4.2) is moved nearer the object, some of the reference beam captured does not interfere with the

object beam. For DIH, we want a hologram where the holographic diffraction is dominant (i.e., the object beam and the reference beam interference is evident).

However, one must be careful in this premise. Note that in the simulations, the intensity of the light source used is not taken into account. As we move the CCD array away from the light source, the light intensity decreases. There is an optimal distance from the CCD array to the light source where there is still enough light intensity and the holographic diffraction is still dominant.

5.1.2 RECONSTRUCTION DISTANCE

A DIH hologram is simulated 15mm from the object plane (Figure 5.1b). The parameters used are the same of that in section 5.1.1. As expected, the reconstruction focuses at the plane where the hologram is simulated (see Figure 5.2). At the right position the image focuses and as we go away from this, the image becomes out of focus. Thus, it is important to know the distance of the object plane to the hologram plane in order to produce a sharp image.

This focusing effect is vital in applications in object localization. This has various applications in fields such as computer vision and robotics, engineering, nanofabrication, super-resolution microscopy and micro-particle characterization [3]. With the use of several numerical focusing characterizations, one may determine the relative distances of objects.

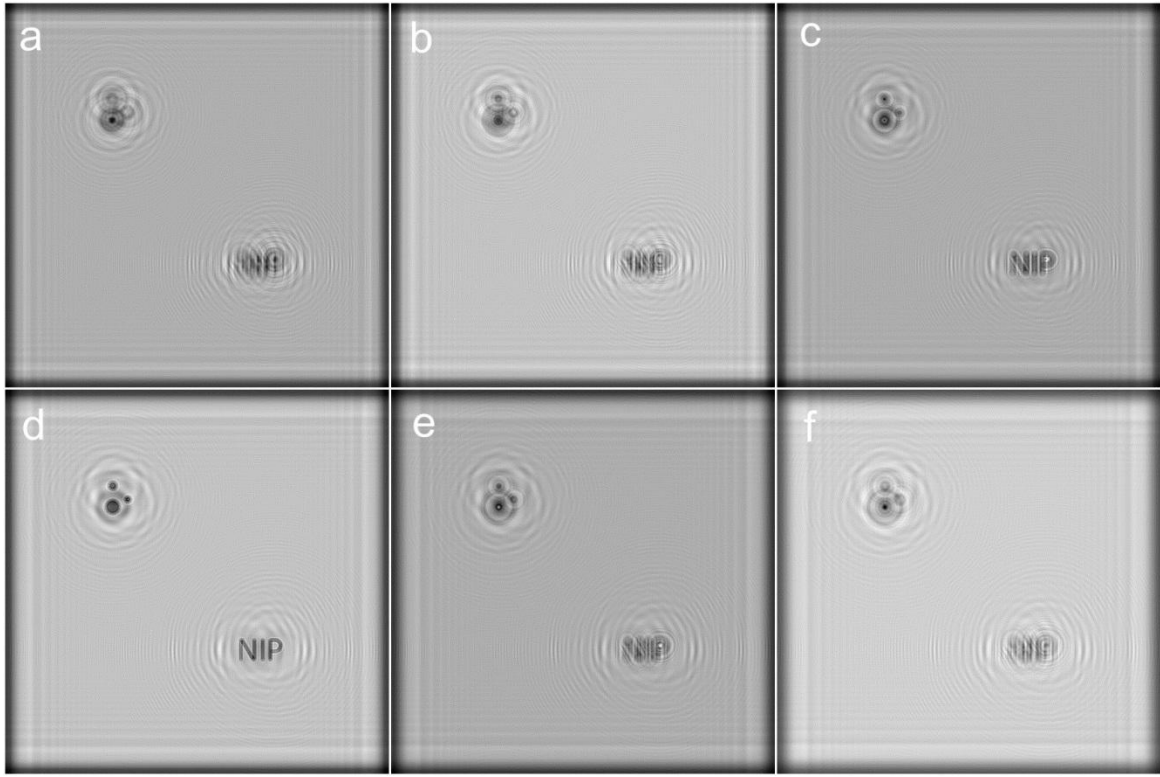


Figure 5.2. Reconstructions of a hologram captured 15mm from the object plane. The reconstruction distances are (a) 9mm, (b) 11mm, (c) 13mm, (d) 15mm, (e) 17mm and (f) 19mm.

The focused reconstruction of the hologram is seen in Figure 5.2d. As one may notice, there are unwanted background fringes. These correspond to the twin-image in DIH. As discussed in section 3.1, this is the distorted real image which is aligned to the viewers' point of view in reconstruction. Several techniques for the suppression of the twin-image have already been presented in literature [2, 4]. An iterative reconstruction algorithm has been initially created for this thesis based on the algorithm presented by X.M. Henry Huang [4]. However, initial results show a divergence problem. The probable cause of such divergence is because the simulated object is a “general” object in contrast with the “pure amplitude” assumption of the paper. The “non-uniqueness” of the solution is cited as the cause for the impossibility of the reconstruction of such. The created algorithm code for this is presented in the appendix as a subroutine function named as `iterate.m` for reference. Future work shall include an iterative algorithm which is able to suppress the twin image in objects with pure phase or the combination of both amplitude and phase.

5.1.3 BACKGROUND FIELD

The test object used is simulated to have a (1) plane wave background with tilt, (2) spherical wave background and (3) plane wave background with no tilt. The phase maps of the object field to be used with the plane wave with tilt and spherical wave is presented in Figure 5.3a and 5.3b, respectively. For the object with the plane wave with no tilt, the image in Figure 4.1a is used.

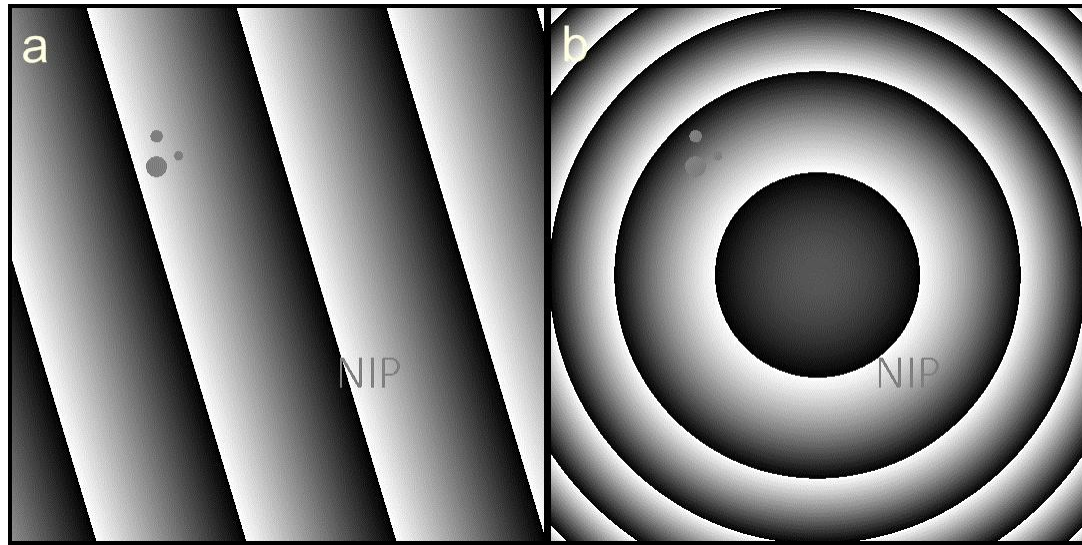


Figure 5.3. The phase map of the objects used. Object with (a) plane wave with tilt and (b) spherical wave.

The holograms are simulated to be at 15mm, with the parameters presented in section 5.1.1. The holograms are reconstructed at 15mm, the distance where the image is the sharpest. From visual inspection of the images (Figure 5.4), it is evident that the reconstructed image without the tilt is the ‘cleanest’. A closer inspection is done by doing a line scan at the 360th pixel of the images as seen in the line in Figure 5.5.

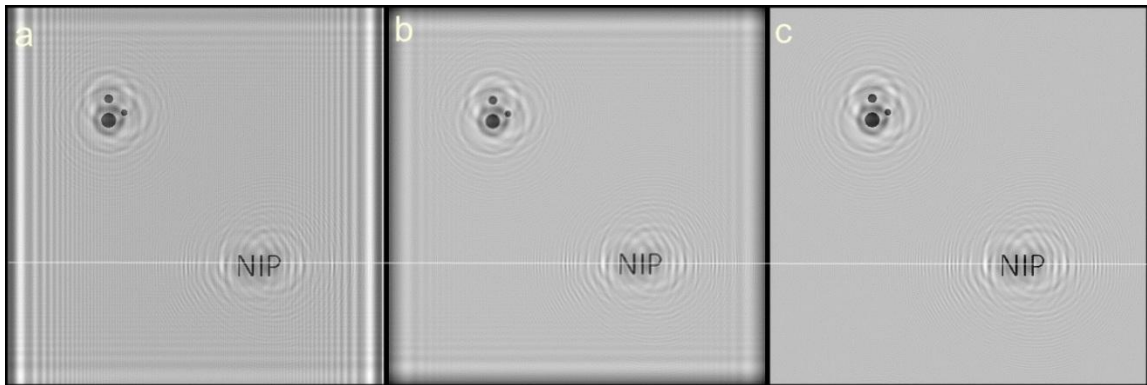


Figure 5.4. Reconstruction of the holograms created with the object having a (a) plane wave with tilt, (b) spherical wave and (c) plane wave without tilt. A line scan is obtained from the images.

Figure 5.5 shows the zoomed line scan (at 360th pixel, vertically) of the images in horizontal pixels 0-200. As one may notice, the red solid line has the least fluctuations. This corresponds to the image to the ‘cleanest’ reconstruction which is the one without the tilt. In Figure 5.6, the part of the image with the lettering NIP is highlighted in the line scan. It is evident that only the red solid line reaches the 0 gray level which corresponds to a black color. Among the three, it also has the lowest dips in the graph. This corresponds to the most focused image among the three. Therefore, the object without the tilt produces the ‘cleanest’ and sharpest reconstruction.

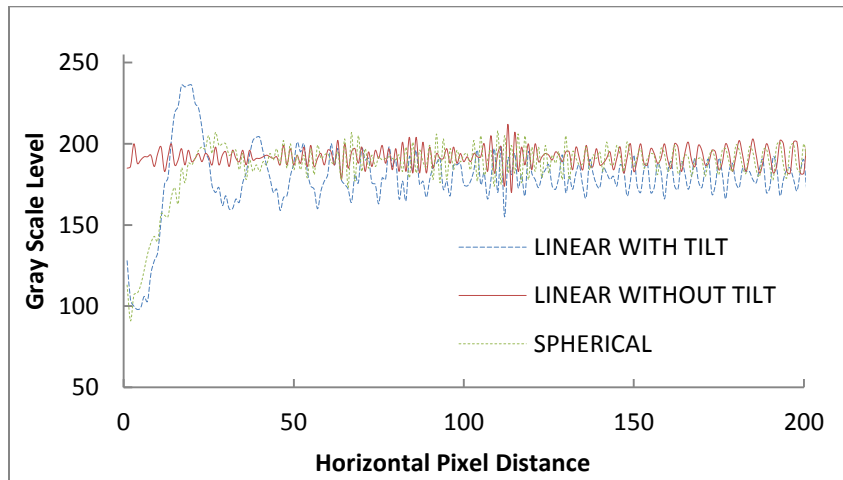


Figure 5.5 Line Scan of the images in Figure 5.5 zoomed in the first 200 pixels of the scan.

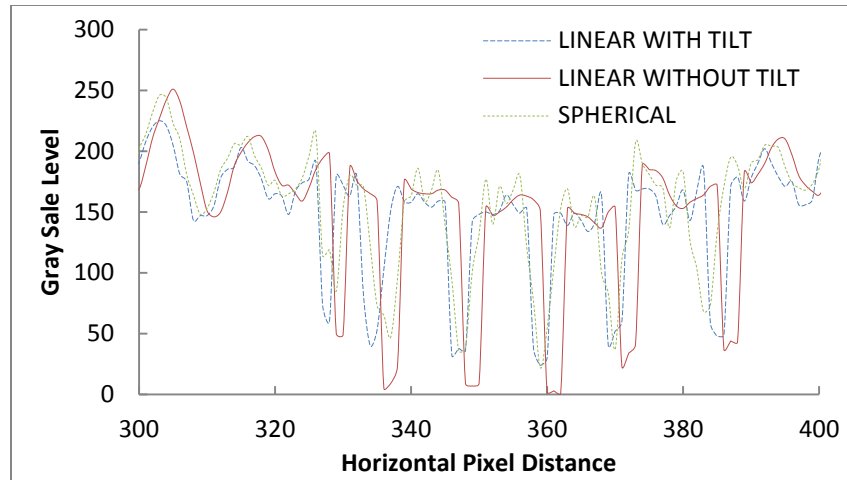


Figure 5.6. Line Scan of the images in Figure 5.5 zoomed in the 300th-400th pixels of the scan. The peaks correspond to the ‘NIP’ object.

A practical implementation of this is the subtraction of the background field with the hologram. This is called the contrast hologram in literature [5]. This does not only create the reconstruction with the ‘cleanest’ and sharpest image but also prevents residual interference fringes and artificial features as seen in [5].

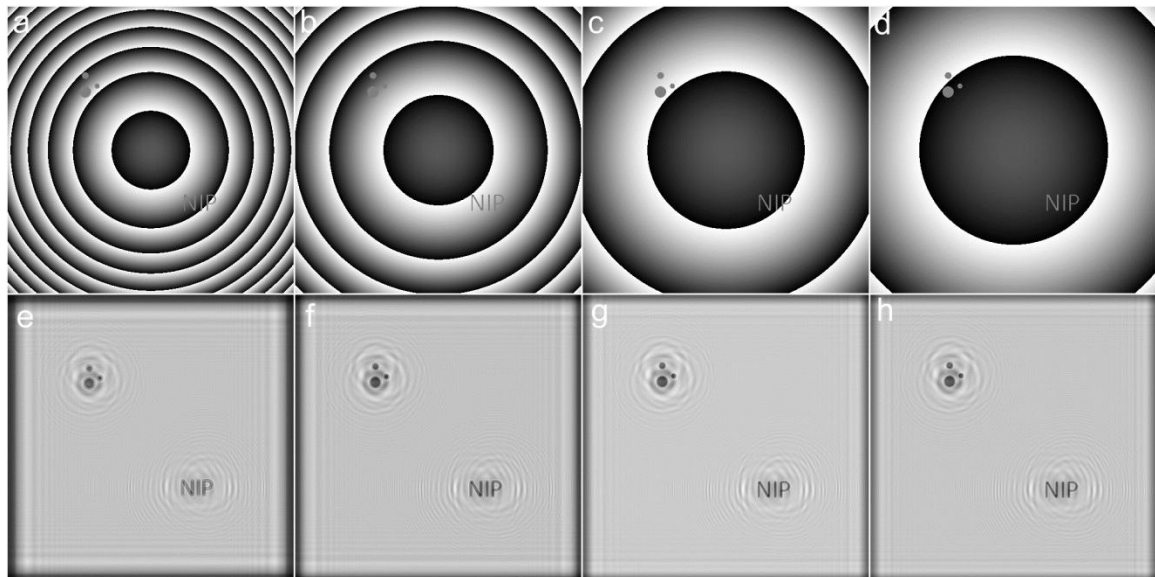


Figure 5.7. Focused images of objects under different degrees of spherical aberrations. (a)-(d) shows the test objects used in the simulations with different degrees of spherical aberrations while (e)-(h) shows the reconstruction in the focused plane.

We also observe the behaviour of the reconstructed image at different degrees of spherical aberrations. As seen in Figure 5.7, as the degree of aberration increases, the quality of the reconstructed image decreases. As one may notice in Figure 5.7e, the lettering of NIP becomes thicker. In comparison with Figure 5.7h, the sharpness of the word NIP is evident. From these results, we may say that a lower degree of aberration creates a sharper image.

5.1.4 WAVELENGTH

Several holograms are created using different wavelengths. The holograms are reconstructed at their respective wavelengths. Figure 5.8 shows the reconstructed holograms using UV light ($\lambda=200\text{nm}$), green light ($\lambda=532\text{nm}$), red light ($\lambda=632\text{nm}$) and infrared light ($\lambda=800\text{nm}$). From the simulation results, the UV light produces the smallest fringes and has the smallest twin-image. Therefore, it has the ‘cleanest’ reconstruction. This is probably because UV light has the shortest wavelength.

We also tested the behaviour of the reconstruction program when the input wavelength is not the same with the actual wavelength used. A hologram is created with 500 nm as the wavelength. Figure 5.9 shows the reconstructed amplitude maps from the hologram. The values used are $\lambda = 200\text{ nm}$, 500 nm and 800 nm . As expected, the correct value ($\lambda=500\text{nm}$) is the sharpest reconstruction. As the value of the wavelength deviates from the actual wavelength used, the reconstructed image becomes defocused.

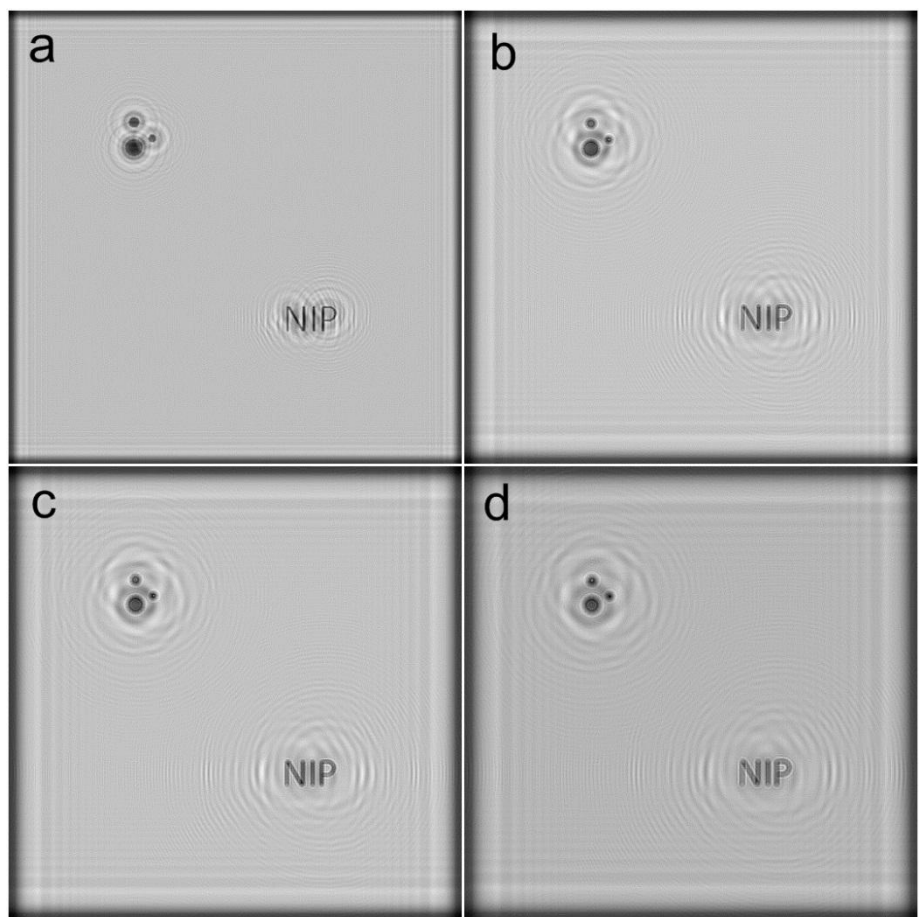


Figure 5.8. Hologram reconstructions under different wavelengths. The holograms are created and reconstructed at the same distances. (a) UV - 200 nm, (b) Green – 532nm, (c) Red – 632nm and (d) Infrared – 800nm.

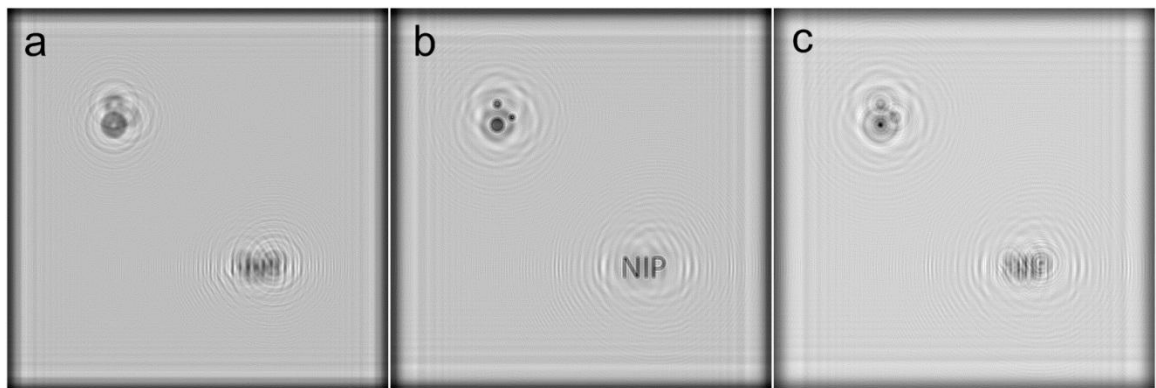


Figure 5.9. Hologram reconstructions under different wavelengths. The holograms are created using $\lambda = 500\text{nm}$ and reconstructed at the same distance but with a different wavelength (a) UV - 200 nm, (b) Green – 500nm, and (c) Infrared – 800nm.

5.2 EXPERIMENTS

5.2.1 REGULAR-SHAPED OBJECTS (GLASS BEADS)

Figure 5.10a shows the hologram of the spherical glass bead samples. The hologram is reconstructed using the developed reconstruction program. Figure 5.10b shows the reconstructed amplitude of the glass beads. It is reconstructed 32mm from the hologram plane. A certain portion (red box) is highlighted to give us a better view of the glass beads.

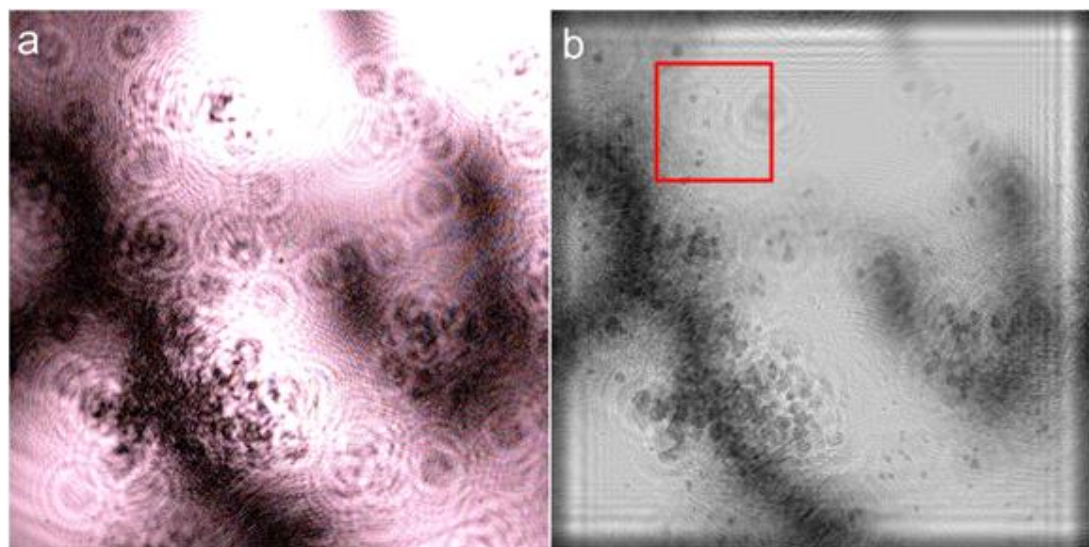


Figure 5.10. The hologram of the glass beads and its reconstruction. The red box in (b) is zoomed in to Figure 5.11.

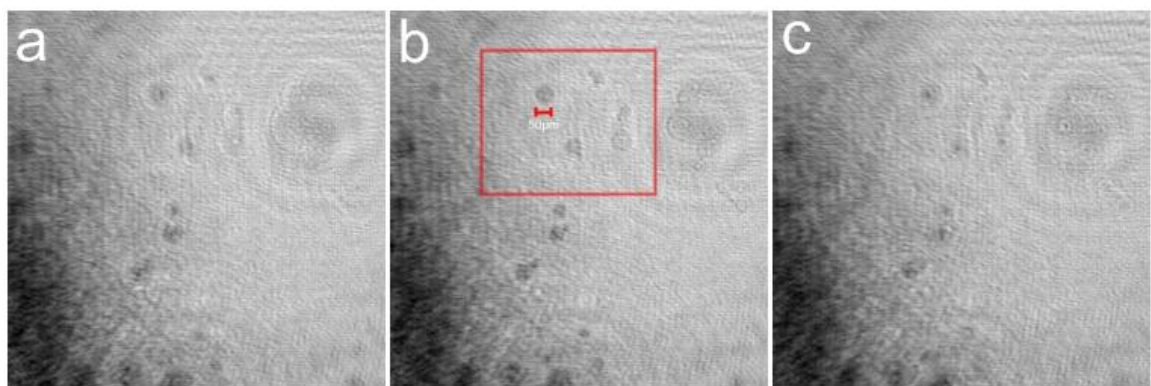


Figure 5.11. The reconstruction of the hologram in Figure 5.10a (glass beads). Reconstruction distance: (a) 30mm, (b) 32 mm and (c) 34mm.

Figure 5.11 shows the highlighted portion in Figure 5.10. The hologram is reconstructed at different distances. In Figure 5.11, it is reconstructed at 30mm, 32mm and

34mm, respectively. It can be shown that at the right reconstruction distance, the glass beads appear to be focused and as the reconstruction distance deviates from the actual distance of the object to the hologram, the images defocus. The manifestation of this focusing effect and the reconstruction of the glass beads indicate the successful implementation of DIH.

5.2.2 IRREGULAR-SHAPED OBJECTS (LIME POWDER)

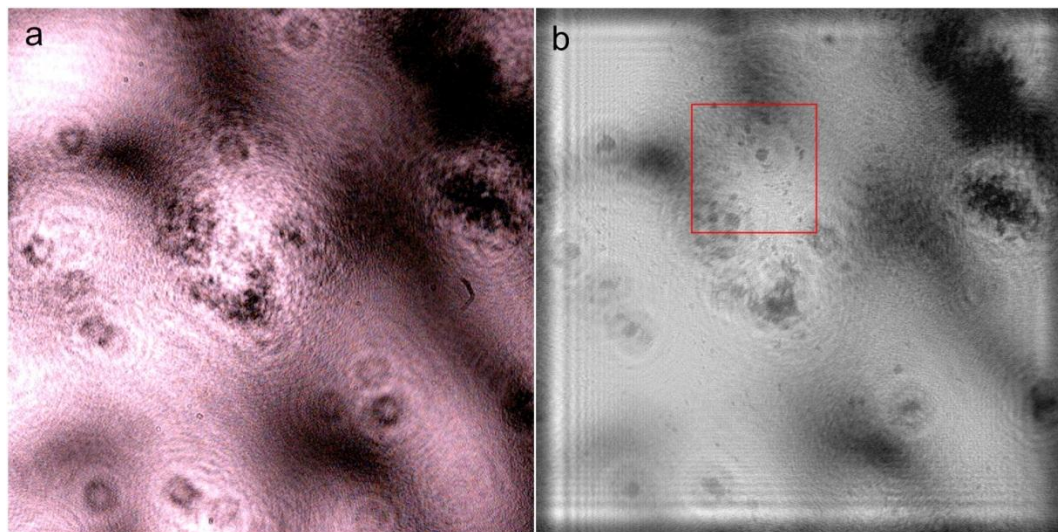


Figure 5.12. The hologram of lime powder and its reconstruction. The red box in (b) is zoomed in to Figure 5.13.

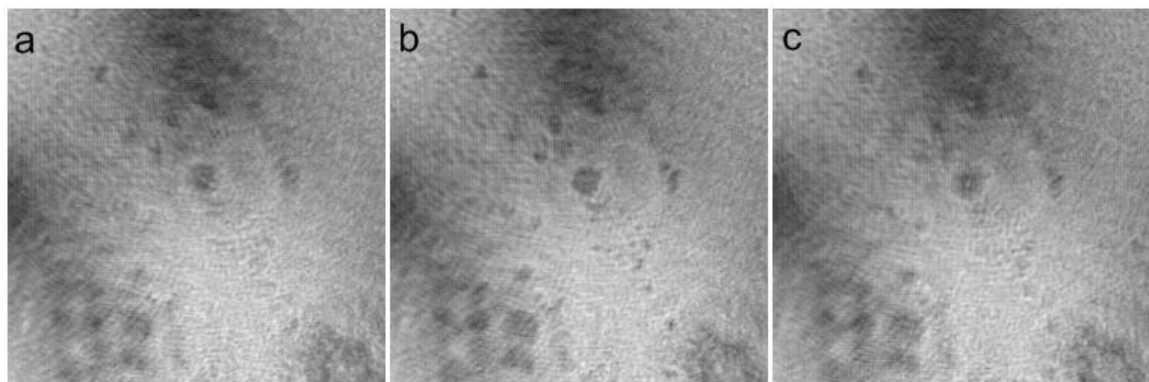


Figure 5.13. The reconstruction of the hologram in Figure 5.12a (lime powder). Reconstruction distance: (a) 28mm, (b) 30 mm and (c) 32mm.

Just like in the previous section (5.2.1), a hologram is captured and reconstructed as seen in Figure 5.12. The hologram reconstruction appears to be the sharpest when it is reconstructed 30mm from the hologram plane. We zoom in a certain portion in the

reconstruction in order to probe the focusing better. As seen in Figure 5.13, the reconstructed image focuses at 30mm and defocuses at other planes. This is a manifestation of the validity of the reconstruction program. This result tells us the effectiveness of the technique even when the sample is irregularly shaped.

5.2.3 BIOLOGICAL SAMPLE (CHEEK CELLS)

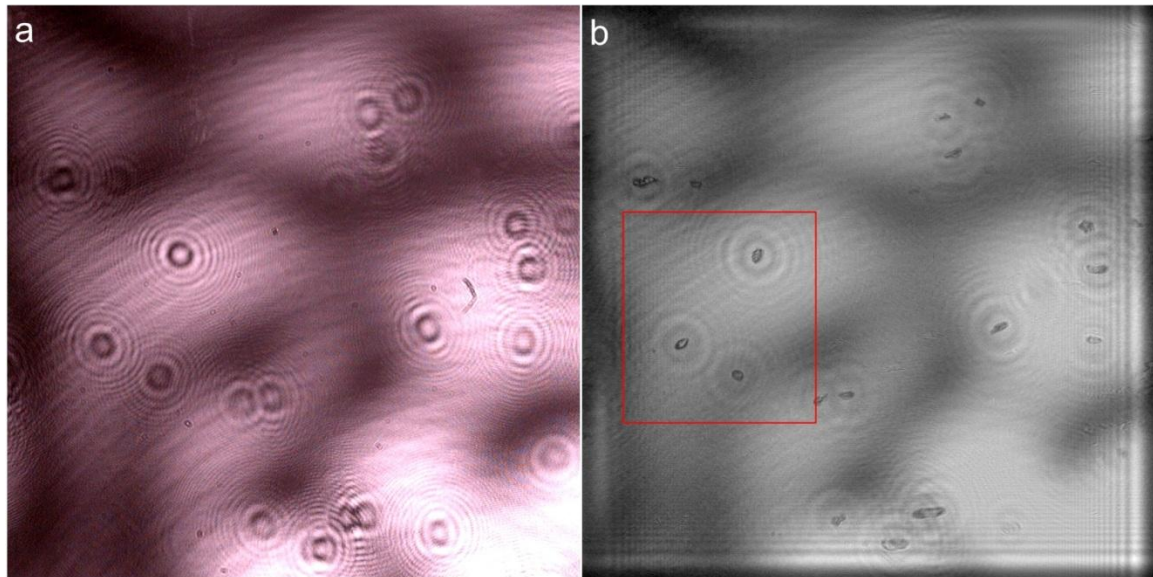


Figure 5.14. The hologram of cheek cells and its reconstruction. The red box in (b) is zoomed in to Figure 5.15.

Figure 5.14 shows the captured hologram of the cheek cells together with its reconstruction on the plane where it is focused. On the other hand, Figure 5.15 shows the evolution of the reconstructed hologram at different planes. This sample is of particular interest because the image focuses at different planes (see Figure 5.15i-k). This means that different parts of the cheek cells are localized. This verifies the ability of DIH to recover the full wave of the object. In Figure 5.15i, the ‘tip’ of the cheek cell is seen and on the next plane (Figure 5.15j) the middle part of the cheek cell is focused. Lastly, on Figure 5.15k, the base of the cheek cell is imaged. Several components of the structures in the cell are seen. Several modifications and further development in the set-up (i.e., introduction of a lens or a larger numerical aperture) may be included in future works to implement the set-up for microscopy.

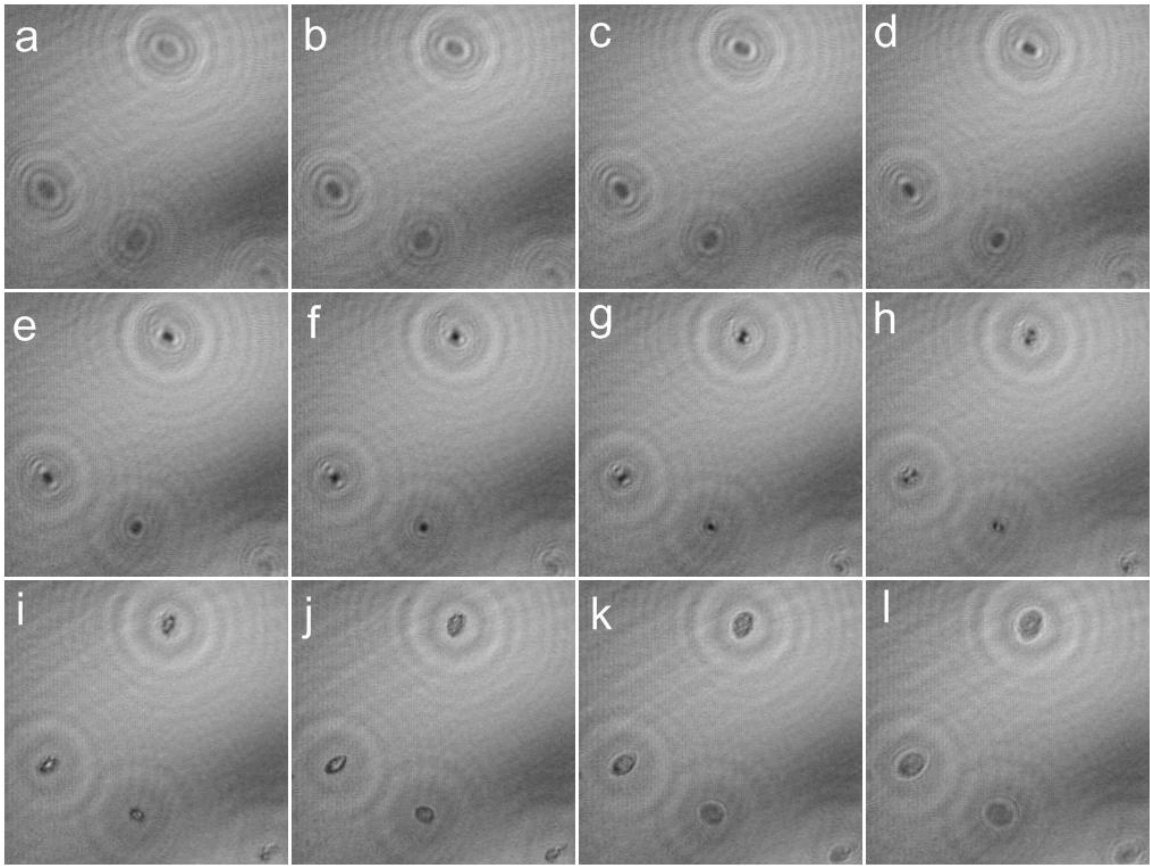


Figure 5.15. The reconstruction of the hologram in Figure 5.14a (cheek cells). Reconstruction distance: (a) 13mm, (b) 14mm, (c) 15mm (d) 16mm, (e) 17mm, (f) 18mm, (g) 19mm, (h) 20mm, (i) 21mm, (j) 22mm, (k) 23mm and (l) 24mm.

5.2.4 AXIAL MOVEMENT MEASUREMENT

Figure 5.16 shows the holograms captured at plane Z_A and plane Z_B , respectively (see Figure 4.3 for the Z_A and Z_B definition). We focus on the part of the holograms with the red box. It may be noticed that the spheres have moved laterally. However, this is not of our concern since we are interested in the axial movement of the spheres. We reconstruct the whole hologram at different planes in order to determine the focused plane.

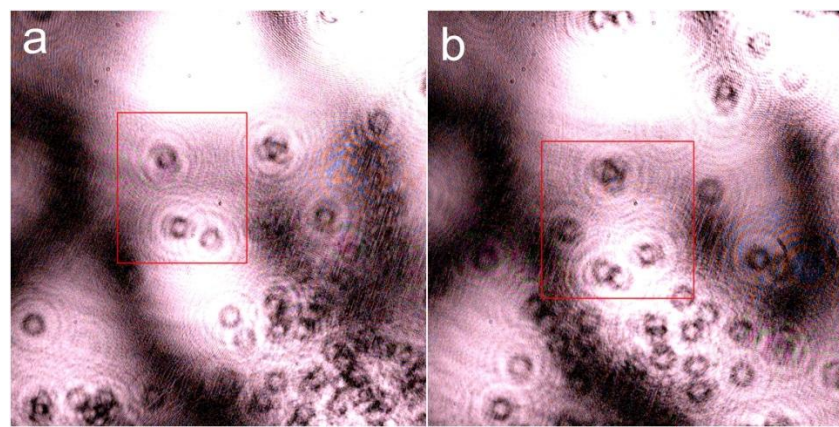


Figure 5.16. Holograms captured for axial measurement. Hologram of the spherical beads at (a) plane Z_A and (b) plane Z_B .

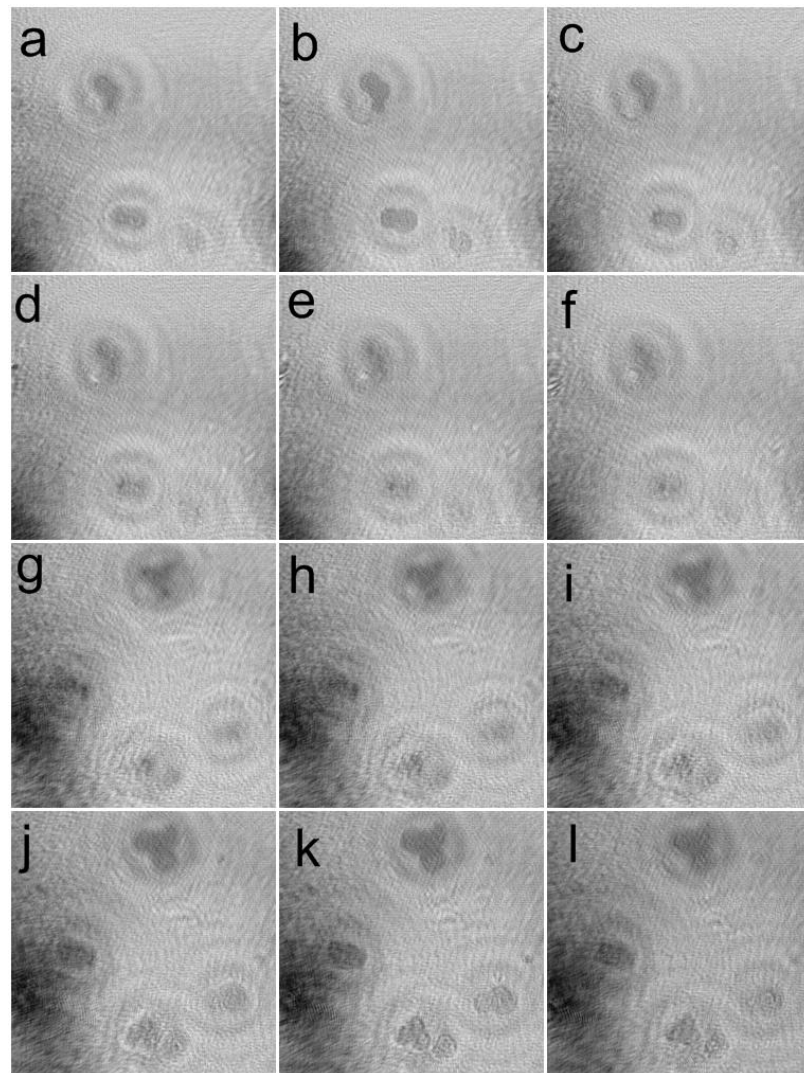


Figure 5.17. Hologram reconstructions at different planes. Reconstruction using the hologram when the object is at plane (a)-(f) Z_A and (g)-(l) Z_B . Distances used is 29mm, 31mm, 33mm, 35mm, 37mm and 39mm, from (a)-(f) and (g)-(l), respectively.

Figure 5.17 shows the reconstruction of the holograms captured in plane Z_A and Z_B . In Figure 5.17(a-f), we can see the evolution of the reconstruction as the plane of reconstruction is varied from 29mm to 39mm. For this set, it is evident the hologram reconstruction focuses at 31mm (Figure 5.17b). For Figures 5.17(g-l), the hologram reconstruction focuses at 37mm (Figure 5.17k). Therefore, we may conclude that the plane Z_A is located 31mm from the hologram while plane Z_B is located 37mm from the hologram. Thus, the axial movement Δz of the spherical beads is 6mm.

5.2.5 OBJECT LOCALIZATION



Figure 5.18. Hologram of the sample with the cheek cells on plane Z_A and the spherical beads on plane Z_B .

The hologram to be used for object localization is seen in Figure 5.18. The cheek cells are placed Z_A from the CCD array while the spherical beads are placed Z_B from the CCD array. We reconstruct this hologram at different planes and focus on a certain area of interest (red box in Figure 5.18). The hologram is reconstructed at distances 11mm to 30mm at 1mm interval as seen in Figure 5.19. At 14mm (Figure 5.18d), the numerical focusing of the spherical beads are already evident (see the red boxes). As we further move the reconstruction plane, we see that at plane 28mm the reconstruction focuses again already. Due to the three dimensional nature of the cheek cell, one may notice that it focuses

at different planes (at 27-29mm). We choose 28mm as the average focused distance of the sample. Since the spherical beads are at 14mm while the cheek cells are 28mm from the hologram, we can conclude that the relative distance between the cheek cells and the spherical beads is 14mm.

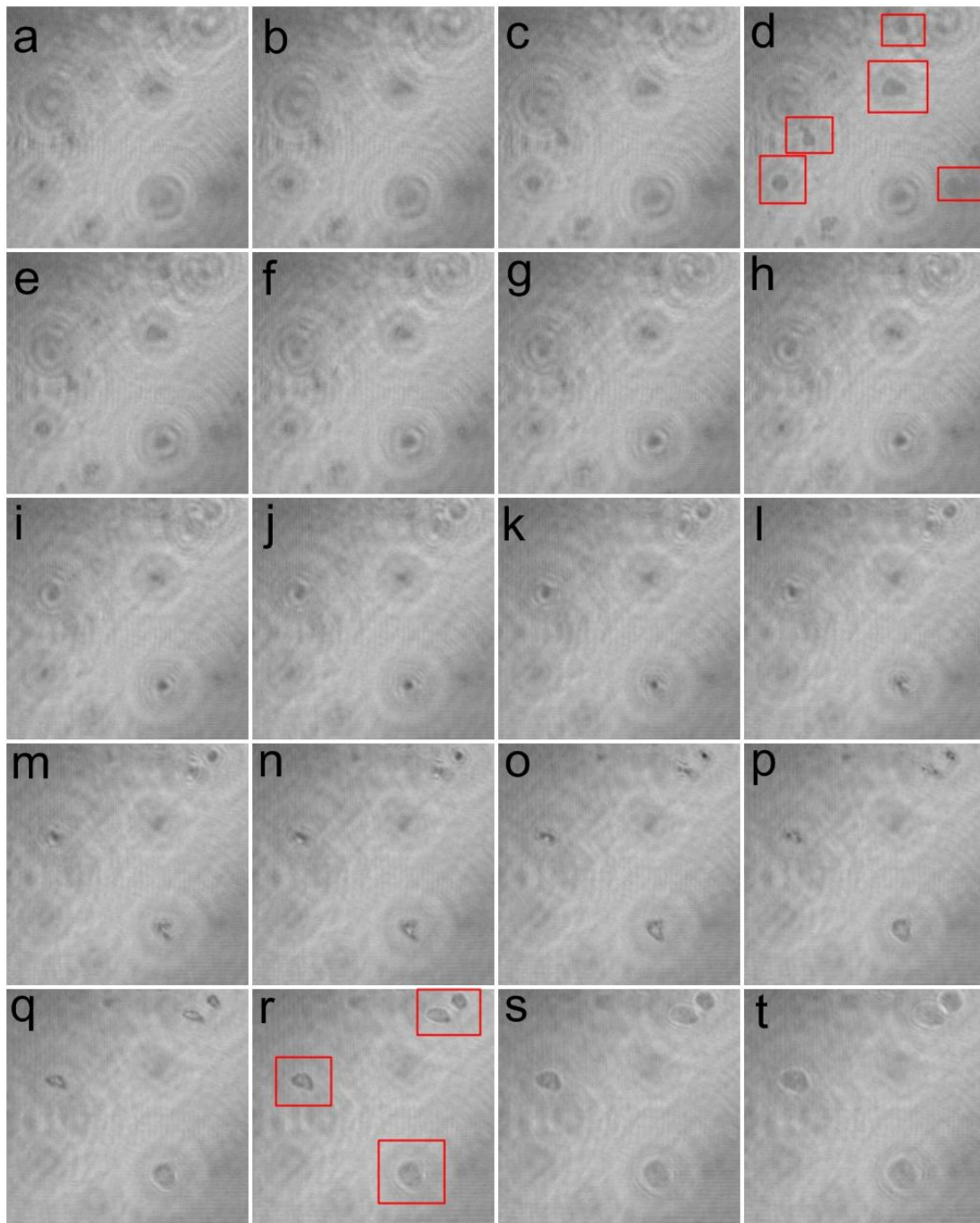


Figure 5.19. Reconstruction of the hologram of the sample with the cheek cells on plane Z_A and the spherical beads on plane Z_B . The distances range from 11mm to 30mm at 1mm intervals. The red boxes show the focused image of the spherical beads and the cheek cells.

REFERENCES

1. L. Repetto, E. Piano and C. Pontiggia, "Lenless digital holographic microscope with light-emitting diode illumination", Opt. Letters 29 (10) pp.1132-1133 (2004).
2. L. Denis, C. Fournier, R. Fournel and C. Duottet, "Numerical suppression of the twin image in in-line holography of a volume of micro-objects", Submitted to Meas. Sci. Technol.
3. V. Gonzales, "Enhanced object localization using axial variation of reconstructed phase maps", NIP Undergraduate Thesis, 2011.
4. X. Huang, J. Zuo and J. Spence, "Wavefront reconstruction for in-line holograms formed by pure amplitude object", Applied Surface Science Vol.148, 1999.
5. P. Ferraro et al. (eds.), Coherent Light Microscopy, Springer Series in Surface Sciences 46, DOI 10.1007/978-3-642-15813-1_1

CHAPTER V: CONCLUSIONS AND RECOMMENDATIONS

This thesis provided a successful implementation of Digital In-line Holography (DIH). A reconstruction program is developed and several parameters are studied through simulations. Several observations are seen:

1. As the distance from the hologram plane and object plane increases, the area of the diffraction pattern in the hologram increases.
2. The reconstruction focuses at the plane where the hologram is simulated. At the right position the image focuses and as we go away from this, the image becomes out of focus.
3. A reconstructed image with no background tilt has the ‘cleanest’ and sharpest image.
4. An object subjected to a lesser degree of aberration gives a sharper image.
5. The use of a shorter wavelength decreases the size of the twin-image in reconstruction.
6. As the value of the wavelength deviates from the actual wavelength used, the reconstructed image becomes defocused.

The reconstruction algorithm is implemented using experimental data. First, the reconstruction program is used to obtain the wavefront of regular objects (spherical glass beads), irregular objects (lime powder) and biological samples (cheek cells). All the three objects were successfully reconstructed. The algorithm is further tested for applications such as axial movement measurement and object localization. For the axial movement measurement, the movement of the spherical beads was obtained to be 6mm. For object localization, the spherical beads and the cheek cells were localized and the relative distance

between the two samples was found to be 14mm. For both applications, the focusing effect of the reconstructed holograms was used.

Further development of this technique and its intersection with other research field in the laboratory is highly recommended. These include:

1. Use of other light sources (i.e., Femto- or nano-second lasers and various LED light)
2. Development of an iterative algorithm for the suppression of twin-image
3. Further discussion on the phase properties as well as its reconstruction in DIH (i.e., development of a multiple plane phase retrieval in DIH)

APPENDIX A

SIMULATION PROGRAM

A.MAIN PROGRAM (main.m)

```
%%Digital In-Line Holography Simulation
%%Based on the FK integral
%%Rommel L. Bartolome
%%Feb. 24, 2013

ij=sqrt(-1);

%% CREATE FIELD

%%AMPLITUDE LOADING
amp = imread('test.png');
amp = im2bw(amp, 0.5);
amp = double(amp);
[M,N] =size(amp);

%%PHASE CREATION
phase = simphaselin(2, amp, 10, -3, 50, 0, 0);
%%phase = ones(size(amp));

%%ACTUAL FIELD CREATION
Z = amp.*exp(ij*(phase));

%%DISPLAY CREATED FIELD
ph=angle(Z);
figure(1);
colormap(gray(256));
mi=min(min(ph));
ph=ph-mi;
fact=256/(max(max(ph)));
ph2=ph*fact;
image(ph2);
axis square;
vv= ['test_',int2str(deg),'.tif'];
%imwrite(uint8(ph2),vv,'tif')

%% INITIALIZATIONS
a_hol=5.2;
lambda_laser=0.6328;
L1=1000;

%% CREATE HOLOGRAM
min_L=15; %%in mm
Hologram = CreatedIH(Z, a_hol, L1, min_L, lambda_laser);

%%DISPLAY HOLOGRAM
```

```

ph=Hologram;
figure(3);
colormap(gray(256));
mi=min(min(ph));
ph=ph-mi;
fact=256/(max(max(ph)));
ph2=ph*fact;
image(ph2);
axis square;
vv= ['holo_',int2str(min_L),'.tif'];
%imwrite(uint8(ph2),vv,'tif')

%% RECONSTRUCT HOLOGRAM
for min_L=9:2:21;
fieldprop = PropagateDIH(Hologram, a_hol, L1, min_L, lambda_laser);

%qmax = 0;
%field = iterate(fieldprop, qmax, a_hol, L1, min_L, lambda_laser);

%%DISPLAY RECONSTRUCTION
ph=abs(fieldprop);
figure(4);
colormap(gray(256));
mi=min(min(ph));
ph=ph-mi;
fact=256/(max(max(ph)));
ph2=ph*fact;
image(ph2);
axis square;
vv= ['rec_15mm_deg_',
int2str(deg), 'mm_reconstruction_',int2str(min_L), '.tif'];
imwrite(uint8(ph2),vv,'tif')
%rms(L1) = corr2(LALA, ph2);
end
%plot(rms, [100:100:1000])

```

B.PHASE SIMULATOR (simphaselin.m)

```

%%Phase simulation program v3.1
%%Rommel Bartolome
%%Jan. 12, 2012

function phase = simphaselin(wavetype, amp, aa, bb, lambda, x_off,
y_off);

ij=sqrt(-1);
[m,n]=size(amp);
holo = zeros([m, n]);
k=2*pi/lambda;

%x_off = 20;
%y_off = 20;

```

```

switch wavetype

    case 1
        for i=1:m,
            for j=1:n,
                fr = ij*k*((i)/aa)+((j)/bb));
                holo(i,j) = double(exp(fr));
            end
        end

    case 2
        h=n/2;
        [X,Y] = meshgrid(-h:h-1,-h:h-1);
        path = (-aa.^2-(X+x_off).^2-(Y-y_off).^2);
        path_x2 = path./max(max(path));
        holo=exp(-ij*(path_x2));
    end

holo_ph=angle(holo);
colormap(gray(256));
ph=holo_ph;
mi=min(min(ph));
ph=ph-mi;
fact=256/(max(max(ph)));
image(ph*fact);
axis square;
phase=holo_ph;

```

C.HOLOGRAM CREATOR (CreateDIH.m)

```

%FUNCTION FOR DIH CREATION v1.0
%Rommel L. Bartolome
%January 14, 2013

function I_hol = CreateDIH(field, a_hol, L1, min_L, lambda_laser);

L1=L1*10^3;
min_L=min_L*10^3;
k=2*pi/lambda_laser;
L2=L1-min_L;

impobject=double(field);
[N,M]=size(impobject);
impobject=impobject(1:N,1:N);

%% DEFINE PLANES
%plane Obj
a_obj=L1/L2*a_hol; %sample interval in plane obj
xvec=-N/2*a_obj:a_obj:(N/2-1)*a_obj; %element N/2+1 has coord 0
yvec=xvec;
[xmat,ymat]=meshgrid(xvec,yvec); %the coord matrices

```

```

objradius=sqrt(xmat.^2+ymat.^2);

%%UNCOMMENT IF 'field' is HOLOGRAM
%plane Hol
hxvec=-N/2*a_hol:a_hol:(N/2-1)*a_hol; %element N/2+1 has coord 0
hyvec=hxvec;
[xmat,ymat]=meshgrid(hxvec,hyvec); %the coord matrices
holradius=sqrt(hxmat.^2+ymat.^2);

%Plane Far
a_far=lambda_laser*L1/(N*a_obj); %sample interval in plane Far
fxvec=-N/2*a_far:a_far:(N/2-1)*a_far; %element N/2+1 has coord 0
fyvec=fxvec;
[fxmat,fymat]=meshgrid(fxvec,fyvec); %the coord matrices
farradius=sqrt(fxmat.^2+fymat.^2);

I_hol=ones(N);

G=L2/L1.*exp(i*k*(L1-L2)).*exp(i*k/2*farradius.^2*(1/L1-1/L2));
Obj_plane=field;%E_obj.*exp(i*k*objradius.^2/(2*L1));
E_hol=exp(-i*k.*holradius.^2/(2*L2)).*ifft2c(G.*fft2c(Obj_plane));
I_hol=abs(E_hol).^2;

```

D. HOLOGRAM RECONSTRUCTION (PropagateDIH.m)

```

%FUNCTION FOR DIH RECONSTRUCTION v1.0
%Rommel L. Bartolome
%January 14, 2013

function newfield = PropagateDIH(field, a_hol, L1, min_L,
lambda_laser);

L1=L1*10^3;
min_L=min_L*10^3;
k=2*pi/lambda_laser;
L2=L1-min_L;

impobject=double(field);
[N,M]=size(impobject);
I_hol=impobject(1:N,1:N);

%% DEFINE PLANES
%plane Obj
a_obj=L1/L2*a_hol; %sample interval in plane obj
xvec=-N/2*a_obj:a_obj:(N/2-1)*a_obj; %element N/2+1 has coord 0
yvec=xvec;
[xmat,ymat]=meshgrid(xvec,yvec); %the coord matrices
objradius=sqrt(xmat.^2+ymat.^2);

%%UNCOMMENT IF 'field' is HOLOGRAM
%plane Hol

```

```

hxvec=-N/2*a_hol:a_hol:(N/2-1)*a_hol; %element N/2+1 has coord 0
hyvec=hxvec;
[hxmat,hymat]=meshgrid(hxvec,hyvec); %the coord matrices
holradius=sqrt(hxmat.^2+hymat.^2);

%Plane Far
a_far=lambda_laser*L1/(N*a_obj); %sample interval in plane Far
fxvec=-N/2*a_far:a_far:(N/2-1)*a_far; %element N/2+1 has coord 0
fyvec=fxvec;
[fxmat,fymat]=meshgrid(fxvec,fyvec); %the coord matrices
farradius=sqrt(fxmat.^2+fymat.^2);

%% PROPAGATION PROPER
F=L1/L2.*exp(i*k*(L2-L1)).*exp(i*k/2*farradius.^2*(1/L2-1/L1));
Hol_plane=sqrt(I_hol).*exp(i*k*holradius.^2/(2*L2)); %%UNCOMMENT IF
'field' is HOLOGRAM
E_obj_revisited=exp(-
i*k.*objradius.^2/(2*L1)).*ifft2c(F.*fft2c(Hol_plane));

newfield = E_obj_revisited;

```

E. ITERATION ROUTINE (iterate.m)

```

% ****
% function iterate
% iterative algorithm to suppress DIH twin image subroutine
% ****
% iteration parameters
% qmax - number of iterations

function field = iterate(field, qmax, a_hol, L1, min_L, lambda_laser);

fieldI = abs(field);
L1=L1*10^6;
min_L=min_L*10^3;
k=2*pi/lambda_laser;
L2=L1-min_L;
L1=L1*10^6;
min_L=min_L*10^3;
k=2*pi/lambda_laser;
L2=L1-min_L;
[N,M]=size(field);

%% DEFINE PLANES
%plane Obj
a_obj=L1/L2*a_hol; %sample interval in plane obj
xvec=-N/2*a_obj:a_obj:(N/2-1)*a_obj; %element N/2+1 has coord 0
yvec=xvec;
[xmat,ymat]=meshgrid(xvec,yvec); %the coord matrices
objradius=sqrt(xmat.^2+ymat.^2);

%%UNCOMMENT IF 'field' is HOLOGRAM
%plane Hol

```

```

hxvec=-N/2*a_hol:a_hol:(N/2-1)*a_hol; %element N/2+1 has coord 0
hyvec=hxvec;
[hxmat,hymat]=meshgrid(hxvec,hyvec); %the coord matrices
holradius=sqrt(hxmat.^2+hymat.^2);

%Plane Far
a_far=lambda_laser*L1/(N*a_obj); %sample interval in plane Far
fxvec=-N/2*a_far:a_far:(N/2-1)*a_far; %element N/2+1 has coord 0
fyvec=fxvec;
[fxmat,fymat]=meshgrid(fxvec,fyvec); %the coord matrices
farradius=sqrt(fxmat.^2+fymat.^2);

for q=1:qmax

F=L2/L1.*exp(i*k*(L1-L2)).*exp(i*k/2*farradius.^2*(1/L1-1/L2));
Obj_plane=abs(field).*exp(i*k*objradius.^2/(2*L1));
E_hol=exp(-i*k.*holradius.^2/(2*L2)).*ifft2c(F.*fft2c(Obj_plane));
I_hol=abs(E_hol).^2;

%intensity(q)=E_hol(100).*conj(E_hol(100));
%rms(q)=norm(intensity(q)-fieldI)/(sqrt(q));

F=L1/L2.*exp(i*k*(L2-L1)).*exp(i*k/2*farradius.^2*(1/L2-1/L1));
Hol_plane=sqrt(fieldI).*exp(i.*angle(E_hol)).*exp(i*k*holradius.^2/(2*L2)); %%UNCOMMENT IF 'field' is HOLOGRAM
field=exp(-i*k.*objradius.^2/(2*L1)).*ifft2c(F.*fft2c(Hol_plane));

end

```

APPENDIX B

RECONSTRUCTION PROGRAM

```
%% DIGITAL IN-LINE HOLOGRAPHY RECONSTRUCTION
%% JANUARY 13, 2013
%% ROMMEL L. BARTOLOME

clear all;
ij=sqrt(-1);

%% INITIALIZATIONS
a_hol=5.2;
L1=1000;
lambda_laser=0.6328;

holo_intensity=double(imread('2_loc.bmp'));
Hologram = holo_intensity;

%% RECONSTRUCT HOLOGRAM
for min_L=1:1:50,

    field = PropagateDIH(Hologram, a_hol, L1, min_L, lambda_laser);
    %qmax = 1;
    %field = iterate(Hologram, qmax, field, a_hol, L1, min_L,
    %lambda_laser);

    %DISPLAY RECONSTRUCTION
    ph=abs(field);
    figure(4);
    colormap(gray(256));
    mi=min(min(ph));
    ph=ph-mi;
    fact=256/ (max(max(ph)));
    ph2=ph*fact;
    image(ph2);
    vv=['2_loc',int2str(min_L),'.bmp'];
    imwrite(uint8(ph2), vv, 'bmp');
    axis square;
end
```